Geophys. J. Int. (2000) **141,** 321–336

Characterization of the magnetotelluric tensor in terms of its invariants

J. T. Weaver,[1] A. K. Agarwal[1] and F. E. M. Lilley[2]

[1] *School of Earth and Ocean Sciences, University of Victoria, Victoria BC, Canada,* V8W 3P6. *E-mail: weaver@phys.uvic.ca*
[2] *Research School of Earth Sciences, The Australian National University, Canberra* ACT 0200, *Australia*

Accepted 1999 November 18. Received 1999 November 18; in original form 1998 July 23

SUMMARY

The magnetotelluric impedance tensor is defined in terms of seven independent parameters that are invariant under a rotation of the horizontal axes on the surface of the Earth, plus an angle that defines the orientation of the axes of reference. The invariants are algebraically related to but nevertheless different from those recently proposed by Szarka & Menvielle (1997). They have been chosen in such a way as to have clear representations on a Mohr circle diagram and also to reveal geoelectric properties of the Earth near the site where the impedance data are measured. The first two invariants define the properties of a 1-D earth when the next four invariants are negligibly small. If the next two are also non-negligible, the earth is 2-D with a strike direction that can be recovered. The last three invariants indicate different degrees of three-dimensionality and the discussion of them with reference to small-scale galvanic distortion in an otherwise 1- or 2-D structure largely retraces the insightful pioneering work of Bahr (1988). The properties of the invariants are illustrated with numerical calculations for a synthetic model consisting of a small conductive anomaly in the form of a cube at the surface of an otherwise 2-D earth that is divided by a vertical fault into regions with a strong resistivity contrast. Results are presented for synthetic data that contain only numerical noise, and for data to which 2 per cent random Gaussian noise has been added. The theoretical properties of the invariants are verified by the pure numerical data, and are confirmed statistically by the noisy data.

Key words: electromagnetic induction, impedance tensor, invariants, magnetotellurics, skew.

1 INTRODUCTION

Rotational invariants of the magnetotelluric (MT) impedance tensor have long been used to provide information about the geoelectric structure underlying the sites where impedance data are measured. Well-known examples are the Berdichevsky and determinant impedances (Berdichevsky & Dmitriev 1976; Ranganayaki 1984; Ingham 1988; Park & Livelybrooks 1989), which were introduced to represent in some sense an 'average impedance' from which a 1-D interpretation of the structure could be deduced. Others are the skew parameter of Swift (1967), which has been widely applied to MT data to determine whether the underlying structure can have a 2-D interpretation, and the phase-sensitive skew of Bahr (1988), which indicates whether the data can be attributed to distortions caused by a small localized anomaly or are associated with a truly 3-D regional structure.

Fischer & Masero (1994) have argued that since the 2×2 impedance tensor is complex valued, it should possess eight real invariants corresponding to the eight real elements defining the tensor. They were able to identify seven invariants including one less familiar in magnetotellurics—the Frobenius norm—and concluded that the eighth parameter was associated with the orientation of the axes in which the tensor was expressed relative to principal axes. Their arguments were illustrated geometrically by reference to the ellipses traced out by the tensor components in the complex plane as the axes of measurement rotate (Word *et al.* 1971; Eggers 1982).

Following the approach suggested by Fischer & Masero (1994), Szarka & Menvielle (1997), henceforth referred to as S–M, have recently analysed the rotational properties of the impedance tensor in great detail, and have systematically examined the algebraic relations between the various invariants that had been previously introduced. They also proved that there are indeed seven mutually independent invariants in terms of which all other invariants can be expressed, and that three of them, rather than just two as previously thought (Fischer & Masero 1994), are associated with the determinant of the impedance tensor. Two such sets of seven independent invariants, one called the 'magnetotelluric set' and the other a

'mathematical set', were selected by S–M as those playing fundamental roles, the choice depending on whether one wished to follow historical practice in MT studies or mathematical tradition. For a geometrical illustration of their results, S–M chose to use the Mohr circle diagrams first introduced by Lilley (1976, 1993a,b,c) as an alternative method of representing MT data graphically. They are particularly illuminating in this context because rotational invariants are immediately identified as fixed geometrical properties of the Mohr circles.

The aim of this paper is to consolidate the various approaches to an interpretation of the impedance tensor into a single treatment. First we argue that, in our opinion, the Mohr circle is the preferred graphical representation of an impedance tensor because it is the natural generalization of the simplest representation of a complex-valued *vector* in a plane. We then introduce a set of seven independent invariants that are different from but related to the invariants derived by Fischer & Masero (1994) and S–M. All of them are associated with invariant properties of the Mohr circles, which not only makes their mutual independence geometrically obvious, but also clearly reveals their relationship to the various invariants proposed by other authors. The invariants are chosen in such a way as to have a physical interpretation that allows one to assess the properties of impedance tensors, including those that have been affected by galvanic distortion in the manner elaborated by Bahr (1988) and Groom & Bailey (1989), whatever the orientation of the axes in which they have been measured. The paper concludes with some applications to synthetic data generated by a 3-D modelling program.

2 INVARIANTS OF THE MT TENSOR

In MT investigations the measured data are usually made available as the real and imaginary parts of a (frequency-dependent) tensor $\mathbf{M}$ defined by

$$\mathbf{e}=\mathbf{M}\cdot\mathbf{b}, \tag{1}$$

where $\mathbf{e}\exp(i\omega t)$ and $\mathbf{b}\exp(i\omega t)$ are, respectively, the horizontal electric and magnetic fields of angular frequency ω, recorded at some site on the Earth's surface at time t. Many writers prefer to deal with the impedance tensor $\mathbf{Z}=\mu_0\mathbf{M}$ instead (μ_0 is the permeability of free space), and write the defining equation as $\mathbf{e}=\mathbf{Z}\cdot\mathbf{h}$, where $\mathbf{h}$ is the horizontal magnetic intensity measured in A m^{-1}. However, since measurements of magnetic variations are generally quoted in nT, i.e. units of $\mathbf{b}$, we prefer to work with eq. (1) while avoiding the unfortunate but not uncommon practice of using the misnomer 'impedance tensor' to describe $\mathbf{M}$. We call $\mathbf{M}$ the 'magnetotelluric tensor' or simply the MT tensor. It is assumed that any physically meaningful MT tensor has a non-vanishing determinant with, in particular, its imaginary part non-vanishing. (The need for this assumption is clear from a consideration of the simplest possible problem of induction in a homogeneous earth.)

Let x- and y-axes on the surface ($z=0$) of the earth define the directions of north and east respectively. The positive z-axis points downwards into the earth. Then in the notation of linear algebra, with $\mathbf{M}$ represented by its 2×2 complex-valued matrix M, and the fields $\mathbf{e}$ and $\mathbf{b}$ by the column vectors e and b, eq. (1) becomes $\mathsf{e}=\mathsf{M}\mathsf{b}$, or

$$\begin{pmatrix}\mathsf{e}_1\\ \mathsf{e}_2\end{pmatrix}=\begin{pmatrix}\mathsf{M}_{11} & \mathsf{M}_{12}\\ \mathsf{M}_{21} & \mathsf{M}_{22}\end{pmatrix}\begin{pmatrix}\mathsf{b}_1\\ \mathsf{b}_2\end{pmatrix}. \tag{2}$$

A rotation of the (x, y) axes through an angle θ in a right-handed sense about the positive z-axis is represented by the rotation matrix

$$\mathsf{R}_\theta=\begin{pmatrix}\cos\theta & \sin\theta\\ -\sin\theta & \cos\theta\end{pmatrix}, \tag{3}$$

application of which to eq. (2) yields new vectors e' and b', where

$$\mathsf{e}'=\mathsf{R}_\theta\mathsf{e}=\mathsf{R}_\theta\mathsf{M}\mathsf{R}_\theta^{\mathrm{T}}\mathsf{R}_\theta\mathsf{b}=\mathsf{M}'\mathsf{b}', \quad \mathsf{M}'=\mathsf{R}_\theta\mathsf{M}\mathsf{R}_\theta^{\mathrm{T}}. \tag{4}$$

Here R^{T} is the transpose of R. In the notation of Weaver (1994), the components of M' are

$$\mathsf{M}'_{11}=\zeta_1+\zeta_2\sin 2\theta+\zeta_3\cos 2\theta, \tag{5}$$

$$\mathsf{M}'_{12}=\zeta_4-\zeta_3\sin 2\theta+\zeta_2\cos 2\theta, \tag{6}$$

$$\mathsf{M}'_{21}=-\zeta_4-\zeta_3\sin 2\theta+\zeta_2\cos 2\theta, \tag{7}$$

$$\mathsf{M}'_{22}=\zeta_1-\zeta_2\sin 2\theta-\zeta_3\cos 2\theta, \tag{8}$$

where we have defined

$$\zeta_1=\xi_1+i\eta_1=\frac{1}{2}(\mathsf{M}_{11}+\mathsf{M}_{22}), \tag{9}$$

$$\zeta_2=\xi_2+i\eta_2=\frac{1}{2}(\mathsf{M}_{12}+\mathsf{M}_{21}), \tag{10}$$

$$\zeta_3=\xi_3+i\eta_3=\frac{1}{2}(\mathsf{M}_{11}-\mathsf{M}_{22}), \tag{11}$$

$$\zeta_4=\xi_4+i\eta_4=\frac{1}{2}(\mathsf{M}_{12}-\mathsf{M}_{21}), \tag{12}$$

so that the matrix representation of the MT tensor takes the form

$$\mathsf{M}=\begin{pmatrix}\xi_1+\xi_3 & \xi_2+\xi_4\\ \xi_2-\xi_4 & \xi_1-\xi_3\end{pmatrix}+i\begin{pmatrix}\eta_1+\eta_3 & \eta_2+\eta_4\\ \eta_2-\eta_4 & \eta_1-\eta_3\end{pmatrix}.$$

For convenience later, it is also useful to introduce the dimensionless variables

$$d_{ij}=\frac{\xi_i\eta_j-\xi_j\eta_i}{(\xi_4^2+\xi_1^2)^{1/2}(\eta_4^2+\eta_1^2)^{1/2}}, \tag{13}$$

$$s_{ij}=\frac{\xi_i\eta_j+\xi_j\eta_i}{(\xi_4^2+\xi_1^2)^{1/2}(\eta_4^2+\eta_1^2)^{1/2}}. \tag{14}$$

In their recent paper, S–M identified seven independent real invariants of the matrix M under such rotations. Those that they called the 'magnetotelluric invariants' (to differentiate them from an alternative, largely intersecting set of 'mathematical invariants') are ξ_1 and η_1, ξ_4 and η_4, $\det(\mathscr{R}e\,\mathsf{M})$ and $\det(\mathscr{I}m\,\mathsf{M})$, and $\mathscr{I}m(\det\mathsf{M})$. Here, we shall refer to them as the 'S–M invariants'. Their invariance can be verified directly by manipulating eqs (5)–(8), although the first and third pairs are already well-known invariants of any matrix—its trace and determinant. The second pair, ξ_4 and η_4, are pseudoscalars; that is, they are invariant under rotations but change sign when the axes are inverted. When multiplied by μ_0, they give the arithmetic mean of the two principal impedances in a strictly 2-D model, which is sometimes called the Berdichevsky impedance. We shall assume, therefore, that $\zeta_4\neq 0$ (i.e. $\mathsf{M}'_{12}\neq\mathsf{M}'_{21}$) in any discussion involving 1-D or 2-D models. The final invariant provides a connection between the real and

imaginary parts of M, unlike the other six invariants, which involve exclusively either the real or the imaginary parts, but not both together.

The complex-valued matrix M is defined by the eight real elements $\mathscr{R}e\,\mathsf{M}_{ij}$ and $\mathscr{I}m\,\mathsf{M}_{ij}$, $i=1, 2$; $j=1, 2$. It can therefore be expressed in terms of the seven invariants listed above plus one other parameter still to be determined. Now it is obviously not possible to write down the matrix in full unless one first sets up a coordinate frame in which one can give specific values to the matrix elements. The chosen frame, be it the original one aligned north/east or some other rotated frame, can be defined by a single parameter, for example by the angle between its x-axis and some fixed direction associated with the matrix, and it is this parameter that completes the definition of M. Thus the MT tensor can be uniquely characterized by the seven independent invariants of its matrix M plus one angle that serves to fix the coordinate axes in which the components of the tensor are expressed.

Various other invariants have been proposed from time to time, such as the aforementioned Frobenius norm, the central impedance of Lilley (1993c) and the sum of the squared components of the MT tensor, which belongs to the set of 'mathematical invariants' introduced by S–M. They can all be expressed in terms of the seven S–M invariants listed above.

3 GRAPHICAL REPRESENTATION

It is instructive to discuss first the graphical representation of a complex-valued *vector* in 2-space such as the horizontal electric field **e**. Writing $\mathbf{e}=\mathbf{u}+i\mathbf{v}$, we can simply represent **e** by two distinct vectors **u** and **v** in the x–y plane, as shown in Fig. 1(a). The complex-valued vector **e** is thus defined in terms of the four real components u_x, u_y, v_x and v_y, and there are three obvious invariants under a rotation of the axes, namely the lengths of the two vectors, and the angle ψ between them (Fig. 1a). The last invariant can be expressed in the form of $\cos\psi$, and therefore in terms of **u** and **v** themselves, through

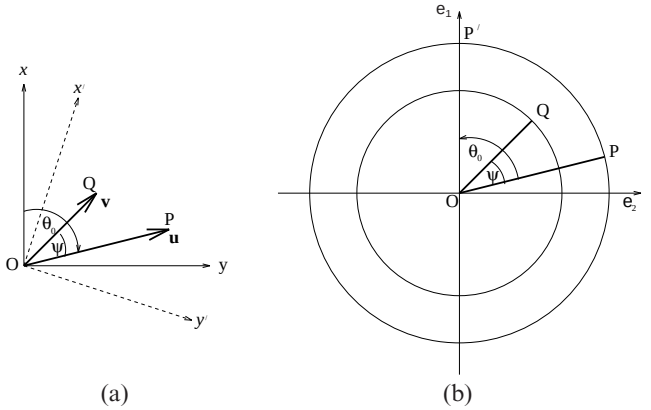

Figure 1. Two representations of a complex vector $\mathbf{e}=\mathbf{u}+i\mathbf{v}$: (a) traditional and (b) algebraic. In (a) rotated (x', y') axes are shown with broken lines, and in (b) points P and Q represent the vectors **u** and **v** respectively referred to the (x, y) axes in (a). As these axes rotate clockwise, the points P and Q trace out the respective 'real' and 'imaginary' circles in a counterclockwise direction, as shown. θ_0 is the angle through which the (x, y) axes must be rotated in order to maximize u_1'. Note that in accordance with geomagnetic convention, the usual directions of the x and y axes have been interchanged in this diagram.

the formula

$$\cos\psi=\frac{(\mathbf{u}\cdot\mathbf{v})}{(\mathbf{u}\cdot\mathbf{u})^{1/2}(\mathbf{v}\cdot\mathbf{v})^{1/2}}\,. \tag{15}$$

An alternative type of representation, which is more in keeping with our algebraic approach, is to fix e_1 and e_2 axes and to plot the values $(\mathsf{u}_1', \mathsf{u}_2')$ and $(\mathsf{v}_1', \mathsf{v}_2')$ taken by the real and imaginary parts of e_1 and e_2 as the (x, y) coordinate axes are rotated. In Fig. 1(b) the original positions of the vectors u and v are indicated by the points P and Q respectively. As the north/east coordinate axes in Fig. 1(a) rotate clockwise in the x–y plane, the points P and Q describe circles in the e_1–e_2 plane in a counterclockwise direction. The point at which the x'-axis in Fig. 1(a) is aligned along the vector **u** corresponds to P reaching the point P′ on the e_1-axis in Fig. 1(b). The three invariants—the radii of the two circles corresponding to the lengths of the vectors, and the angle ψ between the radii to the starting points of P and Q, which is the same as the angle ψ in Fig. 1(a)—are again immediately apparent from the diagram.

The fourth parameter required to determine all four components of the complex vector is the angle θ_0, which gives the direction of **u** relative to the prescribed (northward) x-axis in Fig. 1(a), or the starting position of P relative to the axis of e_1 in Fig. 1(b). A more formal definition of θ_0, which does not rely on reference to a diagram, states that it is that angle through which the original axes must be rotated in order to maximize u_1'.

The representation displayed in Fig. 1(b) is easily generalized to a 2×2 matrix. We take M_{12}' and M_{11}' as the fixed axes, and plot the paths traced out in the M_{12}'–M_{11}' plane by the values of $(\mathscr{R}e\,\mathsf{M}_{12}', \mathscr{R}e\,\mathsf{M}_{11}')$ and $(\mathscr{I}m\,\mathsf{M}_{12}', \mathscr{I}m\,\mathsf{M}_{11}')$ as the (x, y) axes of measurement are rotated about the positive z-axis in a right-handed sense. It follows at once from eqs (5) and (6) that

$$(\mathscr{R}e\,\mathsf{M}_{12}'-\xi_4)^2+(\mathscr{R}e\,\mathsf{M}_{11}'-\xi_1)^2=\xi_2^2+\xi_3^2\,, \tag{16}$$

$$(\mathscr{I}m\,\mathsf{M}_{12}'-\eta_4)^2+(\mathscr{I}m\,\mathsf{M}_{11}'-\eta_1)^2=\eta_2^2+\eta_3^2\,, \tag{17}$$

which are clearly circles centred at (ξ_4, ξ_1) and (η_4, η_1) and of radii $(\xi_2^2+\xi_3^2)^{1/2}$ and $(\eta_2^2+\eta_3^2)^{1/2}$ respectively, as shown in Fig. 2. They are, of course, the familiar Mohr circles first introduced into magnetotellurics by Lilley (1976) and more recently studied in great detail (Lilley 1993c, 1998a,b). The slight variation here is that both the real and the imaginary circles have been plotted on the same diagram, thereby revealing with clarity that ψ, the angle between the radii to the starting points P and Q on the respective circles, plays exactly the same role as the corresponding angle for the vectors in Fig. 1(b), and therefore remains invariant as the axes are rotated. The other six invariants are even more obvious from the diagram. They are the four coordinates of the centres of the circles and the two radii.

Following the discussion at the end of Section 2 and the suggested formal definition of θ_0 in Fig. 1(b), we may specify the final parameter required to complete the definition of the complex tensor as that angle θ through which the axes must be rotated in order to maximize $\mathscr{R}e\,\mathsf{M}_{12}'$. Differentiation of the real part of eq. (6) shows that θ_0 satisfies

$$\tan 2\theta_0=-\xi_3/\xi_2\,. \tag{18}$$

It can be identified on the real Mohr circle in Fig. 2 as half the angle between the radial arm to the starting point P and the diameter parallel to the M_{12}'-axis. We shall call the coordinate axes in which $\mathscr{R}e\,\mathsf{M}_{12}'$ is a maximum the 'MT regional axes'.

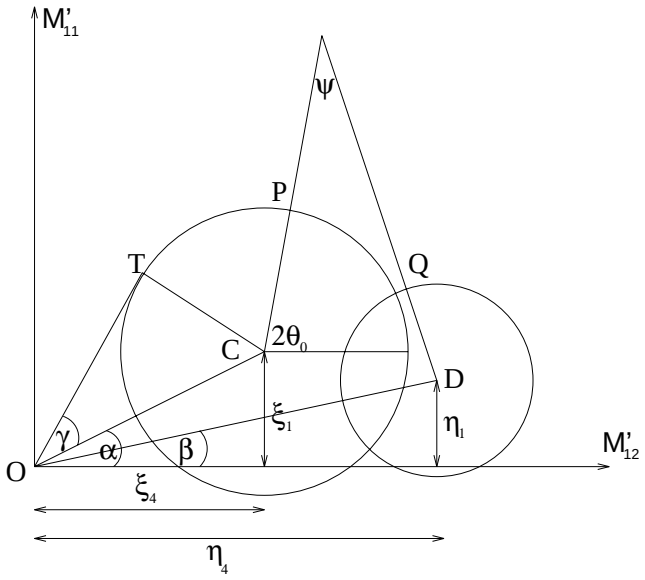

Figure 2. Schematic diagram of real and imaginary Mohr circles, with centres C and D respectively, depicting the 2×2 matrix associated with an MT tensor. θ_0 is the angle through which the original coordinate axes must be rotated in order to maximize $\mathscr{R}e\,\mathsf{M}'_{12}$.

4 A SET OF INDEPENDENT INVARIANTS

Four of the S–M invariants are the coordinates of the centres of the Mohr circles, but the rest are different from the geometrical invariants that have been deduced immediately from Fig. 2. As shown by Lilley (1993c), $[\det(\mathscr{R}e\,\mathsf{M})]^{1/2}$ is the length of the tangent from the origin to the real Mohr circle, or in the right-angled triangle OTC in Fig. 2

$$\det(\mathscr{R}e\,\mathsf{M}) = \xi_4^2 + \xi_1^2 - (\xi_2^2 + \xi_3^2)\,, \tag{19}$$

a result that can be easily verified from formulae (9)–(12). A similar result holds for $[\det(\mathscr{I}m\,\mathsf{M})]^{1/2}$. Thus the third pair of S–M invariants are related to the radii of the Mohr circles and the coordinates of their centres. For their seventh invariant some straightforward algebra with the aid of the definitions (9)–(12) yields

$$\mathscr{I}m(\det \mathsf{M}) = 2(\xi_4\eta_4 + \xi_1\eta_1) - 2(\xi_2\eta_2 + \xi_3\eta_3)\,. \tag{20}$$

In Fig. 2, the invariant $\cos\psi$ linking the real and imaginary circles can be expressed in terms of the two vectors $\overrightarrow{\mathrm{CP}}$ and $\overrightarrow{\mathrm{DQ}}$ by a formula equivalent to (15), in the form

$$\cos\psi = \frac{\xi_2\eta_2 + \xi_3\eta_3}{(\xi_2^2 + \xi_3^2)^{1/2}(\eta_2^2 + \eta_3^2)^{1/2}}\,. \tag{21}$$

To derive this result, we observe, with the aid of (9)–(12), that $\overrightarrow{\mathrm{CP}}$ has components $\mathscr{R}e\,\mathsf{M}_{12} - \xi_4 \equiv \xi_2$ and $\mathscr{R}e\,\mathsf{M}_{11} - \xi_1 \equiv \xi_3$ in the M_{12}–M_{11} plane, and similarly for $\overrightarrow{\mathrm{DQ}}$. For future reference we deduce immediately from (21) that

$$\sin\psi = \frac{\xi_2\eta_3 - \xi_3\eta_2}{(\xi_2^2 + \xi_3^2)^{1/2}(\eta_2^2 + \eta_3^2)^{1/2}} \equiv d_{23}\left[\frac{(\xi_4^2 + \xi_1^2)(\eta_4^2 + \eta_1^2)}{(\xi_2^2 + \xi_3^2)(\eta_2^2 + \eta_3^2)}\right]^{1/2}, \tag{22}$$

the second expression following from definition (13). Note that this formula can yield a negative value for $\sin\psi$ so that it may give the obtuse angle between the vectors $\overrightarrow{\mathrm{CP}}$ and $\overrightarrow{\mathrm{DQ}}$. It follows from (20) and (21) that the final S–M invariant is connected in a relatively obscure manner to the more readily identifiable invariant $\cos\psi$ through the formula

$$\mathscr{I}m(\det \mathsf{M}) = 2\{\xi_4\eta_4 + \xi_1\eta_1 - [(\xi_2^2 + \xi_3^2)(\eta_2^2 + \eta_3^2)]^{1/2}\cos\psi\}\,. \tag{23}$$

The first two terms on the right-hand side of this expression and the factor multiplying $\cos\psi$ are, of course, combinations of previously listed invariants.

Having related the S–M invariants to obvious geometrical invariants that can be read off the Mohr circle diagram, we now ask which set of seven invariants is the most appropriate one to use in MT studies. In seeking such a set we have been guided by three main principles: (i) in general, the invariants should be dimensionless; (ii) each invariant should lend itself to a clear graphical representation on a Mohr circle diagram; and (iii) the vanishing of the invariant should have as simple a physical interpretation as possible. Clearly, none of the S–M invariants satisfy criterion (i), and $\mathscr{I}m(\det \mathsf{M})$ is non-vanishing by definition. In any case, the relative complexity of (23) suggests that any physical interpretation of that invariant would be difficult. Most of the geometrical invariants can be made dimensionless by expressing them in terms of subtended angles rather than coordinates, and they all satisfy criterion (ii), but again some of them do not have simple physical interpretations.

4.1 The fundamental pair

In our view, the fundamental invariants for MT applications should be based on Lilley's (1993c) real and quadrature central impedances. For a real earth model (that is, one that is not perfectly conducting) they are always non-vanishing, and continue to have meaning even when distortions of the electric field by a local anomaly have the effect of making the off-diagonal elements of the impedance tensor equal (i.e. $\xi_4 = \eta_4 = 0$). Since these invariants represent the core of the tensor, there is little point in trying to cast them into a non-dimensional form. We prefer to express them in the dimensions of velocity rather than electrical resistance by dividing the impedance by the factor μ_0 so that the first two invariants are defined as

$$I_1 = (\xi_4^2 + \xi_1^2)^{1/2}, \quad I_2 = (\eta_4^2 + \eta_1^2)^{1/2}\,. \tag{24}$$

These invariants also serve to normalize the remaining invariants. We have already used them in eqs (13) and (14) to make the variables d_{ij} and s_{ij} dimensionless. When the conductivity structure is 1-D ($\zeta_1 = \zeta_2 = \zeta_3 = 0$, $\zeta_4 = \mathsf{M}_{12}$), the familiar parameters of apparent resistivity and phase are given by $\mu_0(I_1^2 + I_2^2)/\omega$ and $\arctan(I_2/I_1)$ respectively.

4.2 Invariants expressing 2-D anisotropy

We would like the next two invariants to express the two-dimensionality of the structure, if relevant. That is, they should vanish when the structure is 1-D, but otherwise contain information about the 2-D anisotropy. A necessary condition of two-dimensionality is that there should exist an angle $\theta = \theta'$ for which the diagonal elements of M' vanish together. From

eqs (5) and (8) we see that the condition $\mathsf{M}'_{11}=\mathsf{M}'_{22}=0$ requires

$$\xi_1=\eta_1=0\,,\quad \tan 2\theta'=-\xi_3/\xi_2=-\eta_3/\eta_2\,, \tag{25}$$

which, by (18), shows that $\theta'=\theta_0+n\pi/2$ (n an integer), that is, the axes are rotated so that they are parallel to the MT regional axes defined in Section 3. (Note that if $\zeta_2=\zeta_3=0$, the angle θ' is not defined, which is to be expected because the structure is then 1-D.) The second statement in (25) also implies $\xi_2\eta_3=\xi_3\eta_2$, or by (22), $\psi=0$. Thus conditions for two-dimensionality can be satisfied geometrically by requiring that the centres C and D of the Mohr circles lie on the M'_{12}-axis, and that the radial arms CP and DQ from the centres of the circles to the starting points on their circumferences are parallel. Given that these conditions hold, the anisotropy is embodied in the radii of the Mohr circles (Lilley 1993c), which in turn are governed by the angles γ and δ between the respective pairs of lines drawn from the origin, tangent to and through the centre of the real and imaginary Mohr circles. The angle γ related to the real Mohr circle has been marked in Fig. 2. Appropriate invariants are therefore

$$I_3=\sin\gamma=\left(\frac{\xi_2^2+\xi_3^2}{\xi_4^2+\xi_1^2}\right)^{1/2}\equiv\frac{(\xi_2^2+\xi_3^2)^{1/2}}{I_1}\,, \tag{26}$$

$$I_4=\sin\delta=\left(\frac{\eta_2^2+\eta_3^2}{\eta_4^2+\eta_1^2}\right)^{1/2}\equiv\frac{(\eta_2^2+\eta_3^2)^{1/2}}{I_2}\,. \tag{27}$$

Note that although the denominators reduce to $|\xi_4|$ and $|\eta_4|$ in a strictly 2-D environment, we have retained the more general forms (26) and (27), which continue to have the simple geometrical interpretation in terms of the angles γ and δ, even when $\zeta_1\neq0$. The values of I_3 and I_4 range from 0 when there is no anisotropy (i.e. when the model is 1-D) to 1 when the anisotropy is extreme (i.e. $|\mathsf{M}'_{21}|/|\mathsf{M}'_{12}|\to0$ or ∞ with respect to the regional axes).

4.3 Three invariants related to galvanic distortion

The remaining invariants should express the three-dimensionality of the structure. It is well known (Lilley 1993c) that when the centres of the Mohr circles depart from the M'_{12}-axis, the structure is 3-D. The invariant angles of inclination of OC and OD with respect to the M'_{12}-axis, α and β respectively, are therefore two of the potential candidates for measuring certain aspects of three-dimensionality. In practice, it is more useful, when defining the next two invariants, to work with the sines of the angles $\beta+\alpha$ and $\beta-\alpha$, which are clearly independent since α and β are. The seventh and final invariant must be related to the remaining independent invariant angle ψ, whose sine is given by (19). Now it is obvious from Fig. 2 that $\tan\alpha=\xi_1/\xi_4$ and $\tan\beta=\eta_1/\eta_4$, so that by definitions (13) and (14) and some simple trigonometry we obtain three independent invariants

$$\sin(\beta+\alpha)=s_{41}\,,\ \sin(\beta-\alpha)=d_{41}\,,\ \sin\psi=d_{23}\csc\gamma\csc\delta\,, \tag{28}$$

which reflect the three-dimensionality of the structure. If $s_{41}=d_{41}=d_{23}=0$ and $\zeta_4\neq0$, then the conditions (25) for two-dimensionality are satisfied.

It is now desirable to ensure that the invariants also have simple physical interpretations. We shall do this by examining the conditions under which it is possible to interpret the three-dimensionality of the MT tensor as originating with distortions of the measured electric field by small-scale anomalies in a regional 1-D or 2-D structure. This assumption, first postulated by Larsen (1977), is fundamental in the various tensor decomposition schemes that have found widespread application in recent years (Zhang *et al.* 1987; Bahr 1988; Groom & Bailey 1989). The anomaly is assumed to be small in size and located at a shallow depth (relative to the inductive scale length in the host medium) so that, over the frequency range of measurement, the regional electric field is essentially uniform and maintains its surface value over the vertical extent of the anomaly. The charges that accumulate on the boundaries of the anomaly and their associated electric fields are therefore in phase with the regional electric field at the surface and are independent of frequency. It is the electric field of these charges that gives rise to the local 'galvanic distortion' of the measured electric field, resulting in the 'channelling' of the regional telluric currents either into the anomaly if it is conductive relative to the regional geology, or around it if it is resistive. It is assumed, however, that the distortion has negligible effect on the regional magnetic field (Agarwal & Weaver 1999).

For convenience in the following discussion we introduce a new invariant,

$$Q=[(d_{12}-d_{34})^2+(d_{13}+d_{24})^2]^{1/2}\,, \tag{29}$$

and note that $Q=0$ if and only if $d_{12}=d_{34}$ and $d_{13}=-d_{24}$. It is not an independent invariant, because by expanding the squared terms under the square root in (29), simplifying algebraically, and substituting from (26), (27) and (28), we find that

$$Q=[\sin^2\gamma+\sin^2\delta-2\sin\gamma\sin\delta\cos(\beta-\alpha-\psi)]^{1/2}\,,$$

which relates the invariance of Q to its dependence on four of the independent invariant angles γ, δ, $(\beta-\alpha)$ and ψ already defined. We note also the identity

$$\begin{aligned}(s_{13}-s_{24})(d_{12}-d_{34})\equiv{}&(d_{13}+d_{24})(s_{12}+s_{34})\\&+d_{41}(s_{22}+s_{33})-d_{23}(s_{44}+s_{11})\,,\end{aligned} \tag{30}$$

which can be verified by reference to the definitions (13) and (14) and some routine algebra. If $Q=0$ and $d_{41}=0$, with $\xi_1\neq0$, $\eta_1\neq0$, $\xi_4\neq0$, $\eta_4\neq0$, i.e.

$$\xi_4\eta_1=\xi_1\eta_4\,,\quad d_{12}=d_{34}\,,\quad d_{13}=-d_{24}\,,\quad s_{41}\neq0\,,$$

then by multiplying the second and third of these equations by ξ_1, replacing the factors $\xi_1\eta_4$ by $\xi_4\eta_1$ as given by the first equation, and finally adding or subtracting the resulting two equations, we obtain $d_{12}=d_{13}=0$. It follows at once that $d_{23}=d_{24}=d_{34}=0$ as well. Furthermore, if $Q=0$ and $d_{41}=d_{23}$, substitution in (30) yields

$$0=d_{41}(s_{44}+s_{11}-s_{22}-s_{33})=d_{41}I_1I_2\,\mathscr{I}m(\det\mathsf{M})\,,$$

the last step following from (20). Since $\mathscr{I}m(\det\mathsf{M})\neq0$ according to our assertion about the physical nature of the impedance tensor at the end of the first paragraph of Section 2, it follows that $d_{41}=0$, which returns us to the conditions discussed above, so that the same conclusions can be drawn. If $s_{41}=0$ as well, then the same results still hold, but if ξ_4 and η_4 remain non-vanishing, we then have $\xi_1=\eta_1=0$, which reproduces conditions (25) for a purely 2-D structure. This case will therefore be disregarded in the discussion of galvanic distortion. (The other possibility, in which $\xi_4=\eta_4=0$ with ξ_1 and η_1 non-vanishing, is a special case briefly mentioned later.)

In summary, if $Q=0$, then $d_{41}=d_{23}$ if and only if $d_{41}=0$ and we may further conclude that $d_{12}=d_{13}=d_{23}=d_{24}=d_{34}=d_{41}=0$. A particular result that follows from these equations is

$$(\xi_4^2+\xi_1^2)(\eta_4^2+\eta_1^2)(\sin^2\gamma-\sin^2\delta)$$
$$=d_{24}s_{24}+d_{34}s_{34}-d_{12}s_{12}-d_{13}s_{13}=0,$$

so that $\sin\gamma=\sin\delta$ or $I_3=I_4$.

Let us suppose that the coordinate axes are rotated, as in (4), into the direction of strike in the regional 2-D structure. The electric field $\mathbf{e}'$ observed in the primed frame of reference is, of course, a distortion of the true regional electric field $\bar{\mathbf{e}}'$, and the corresponding measured MT tensor $\mathbf{M}'$ will not, therefore, take the anti-diagonal form associated with a 2-D structure. That property belongs to the *regional* MT tensor $\bar{\mathbf{M}}'$ defined by $\bar{\mathbf{e}}'=\bar{\mathbf{M}}'\mathbf{b}'$. Here we have used a bar on the symbol to distinguish regional (2-D) values from those actually measured in the primed (rotated) frame of reference. Following Bahr (1988), we may write $\mathbf{e}'=\mathbf{A}\bar{\mathbf{e}}'$, where the matrix $\mathbf{A}$, whose elements, by virtue of the remarks above, are real and frequency-independent, represents the distortion of the electric field in the rotated frame of reference. Smith (1995) expressed the distortion matrix $\mathbf{A}$ in the form

$$\mathbf{A}=\begin{pmatrix} g_1\cos\phi_1 & -g_2\sin\phi_2 \\ g_1\sin\phi_1 & g_2\cos\phi_2 \end{pmatrix}, \tag{31}$$

with the simple physical interpretation that ϕ_1 and ϕ_2 are the angles ranging between $\pm\pi/2$ through which regional electric fields in the x' and y' directions respectively have been rotated positively in the right-handed sense about the z-axis (vertically downwards), and g_1 and g_2 are the 'gains' (or amplifications) they have experienced in undergoing this distortion. It is assumed that $\det\mathbf{A}\neq0$, or equivalently, $g_1\neq0$, $g_2\neq0$ and $|\phi_1-\phi_2|\neq\pi/2$. Alternatively, one can write $\bar{\mathbf{e}}'=\mathbf{D}\mathbf{e}'$, with $\mathbf{D}=\mathbf{A}^{-1}$ representing the matrix that undistorts the measured electric field back into the true regional field. Writing $h=1/g$, we readily deduce from eq. (31) that

$$\mathbf{D}=\begin{pmatrix} h_1\cos\phi_2 & h_1\sin\phi_2 \\ -h_2\sin\phi_1 & h_2\cos\phi_1 \end{pmatrix}\sec(\phi_1-\phi_2). \tag{32}$$

Since $\bar{\mathbf{M}}'\mathbf{b}'=\bar{\mathbf{e}}'=\mathbf{D}\mathbf{e}'=\mathbf{D}\mathbf{M}'\mathbf{b}'$, it follows that $\bar{\mathbf{M}}'=\mathbf{D}\mathbf{M}'=\mathbf{N}\sec(\phi_1-\phi_2)$, where for $j=1,2$

$$\mathbf{N}_{1j}=h_1\cos\phi_2\left[\mathscr{R}e\,\mathbf{M}'_{2j}\left(\tan\phi_2+\frac{\mathscr{R}e\,\mathbf{M}'_{1j}}{\mathscr{R}e\,\mathbf{M}'_{2j}}\right)\right.$$
$$\left.+i\mathscr{I}m\,\mathbf{M}'_{2j}\left(\tan\phi_2+\frac{\mathscr{I}m\,\mathbf{M}'_{1j}}{\mathscr{I}m\,\mathbf{M}'_{2j}}\right)\right], \tag{33}$$

$$\mathbf{N}_{2j}=-h_2\cos\phi_1\left[\mathscr{R}e\,\mathbf{M}'_{1j}\left(\tan\phi_1-\frac{\mathscr{R}e\,\mathbf{M}'_{2j}}{\mathscr{R}e\,\mathbf{M}'_{1j}}\right)\right.$$
$$\left.+i\mathscr{I}m\,\mathbf{M}'_{1j}\left(\tan\phi_1-\frac{\mathscr{I}m\,\mathbf{M}'_{2j}}{\mathscr{I}m\,\mathbf{M}'_{1j}}\right)\right]. \tag{34}$$

Clearly, decomposition of the measured tensor into a 2-D form is possible if and only if $\mathbf{N}_{11}=\mathbf{N}_{22}=0$ when the axes are rotated through some angle $\theta=\theta'$. This condition can only be met if

$$\frac{\mathscr{R}e\,\mathbf{M}'_{11}}{\mathscr{R}e\,\mathbf{M}'_{21}}=\frac{\mathscr{I}m\,\mathbf{M}'_{11}}{\mathscr{I}m\,\mathbf{M}'_{21}},\quad \frac{\mathscr{R}e\,\mathbf{M}'_{22}}{\mathscr{R}e\,\mathbf{M}'_{12}}=\frac{\mathscr{I}m\,\mathbf{M}'_{22}}{\mathscr{I}m\,\mathbf{M}'_{12}}, \tag{35}$$

so that eqs (33) and (34) give

$$\mathbf{N}_{11}=h_1\mathbf{M}'_{21}\cos\phi_2\left[\frac{\mathscr{R}e\,\mathbf{M}'_{11}}{\mathscr{R}e\,\mathbf{M}'_{21}}+\tan\phi_2\right], \tag{36}$$

$$\mathbf{N}_{22}=h_2\mathbf{M}'_{12}\cos\phi_1\left[\frac{\mathscr{R}e\,\mathbf{M}'_{22}}{\mathscr{R}e\,\mathbf{M}'_{12}}-\tan\phi_1\right]. \tag{37}$$

The required decomposition of $\mathbf{M}$ then follows with distortion angles defined by

$$\tan\phi_1=\mathscr{R}e\,\mathbf{M}'_{22}/\mathscr{R}e\,\mathbf{M}'_{12},\quad \tan\phi_2=-\mathscr{R}e\,\mathbf{M}'_{11}/\mathscr{R}e\,\mathbf{M}'_{21}. \tag{38}$$

Eqs (35) state that the arguments (phases) of the complex elements are equal in the first and second columns of $\mathbf{M}'$ respectively, a fundamental property of small-scale galvanic distortion in a 2-D region that was emphasized by Bahr (1988). (More precisely, the arguments could also differ by 180° because, by definition, $-\pi<\arg w\leq\pi$ radians for any complex number w, but this would only have the effect of changing the sign of both the real and imaginary parts so that their ratio remains the same.)

As an aid to considering when conditions (35) can be satisfied, we note the following identities, which are readily verified from eqs (5)–(8) together with definitions (13) and (14):

$$\mathscr{R}e\,\mathbf{M}'_{11}\mathscr{I}m\,\mathbf{M}'_{21}-\mathscr{R}e\,\mathbf{M}'_{21}\mathscr{I}m\,\mathbf{M}'_{11}$$
$$=[(d_{12}-d_{34})\cos2\theta-(d_{13}+d_{24})\sin2\theta+d_{41}-d_{23}]I_1I_2, \tag{39}$$

$$\mathscr{R}e\,\mathbf{M}'_{22}\mathscr{I}m\,\mathbf{M}'_{12}-\mathscr{R}e\,\mathbf{M}'_{12}\mathscr{I}m\,\mathbf{M}'_{22}$$
$$=[(d_{12}-d_{34})\cos2\theta-(d_{13}+d_{24})\sin2\theta-d_{41}+d_{23}]I_1I_2, \tag{40}$$

$$\mathscr{R}e\,\mathbf{M}'_{11}\mathscr{I}m\,\mathbf{M}'_{12}-\mathscr{R}e\,\mathbf{M}'_{12}\mathscr{I}m\,\mathbf{M}'_{11}$$
$$=[(d_{12}+d_{34})\cos2\theta-(d_{13}-d_{24})\sin2\theta-d_{41}-d_{23}]I_1I_2, \tag{41}$$

$$\mathscr{R}e\,\mathbf{M}'_{11}\mathscr{I}m\,\mathbf{M}'_{12}+\mathscr{R}e\,\mathbf{M}'_{21}\mathscr{I}m\,\mathbf{M}'_{22}$$
$$=[(s_{12}+s_{34})\cos2\theta-(s_{13}-s_{24})\sin2\theta-d_{41}-d_{23}]I_1I_2. \tag{42}$$

Identities (39) and (40) show that the equalities (35) hold if either of the conditions

$$d_{12}=d_{34},\quad Q=0,\ \text{i.e. } d_{13}=-d_{24},\quad d_{41}=d_{23}, \tag{43}$$

$$d_{41}=d_{23},\quad Q\neq0,\quad \theta=\theta',\quad \tan2\theta'=\frac{d_{12}-d_{34}}{d_{13}+d_{24}} \tag{44}$$

are satisfied.

We have seen that the conditions in (43) imply $d_{12}=d_{13}=d_{24}=d_{34}=0$, which substituted into eq. (41) gives

$$\mathscr{R}e\,\mathbf{M}'_{11}\mathscr{I}m\,\mathbf{M}'_{12}=\mathscr{R}e\,\mathbf{M}'_{12}\mathscr{I}m\,\mathbf{M}'_{11}. \tag{45}$$

Combined with eqs (35) this result states that the arguments (phases) of *all* the complex elements of $\mathbf{M}'$ are equal or differ by 180°, and this will also be true of $\mathbf{M}$ in the frame of measurement, because (45) holds for any angle θ. Moreover, since the distortion matrix $\mathbf{A}$ is real, the arguments (phases) of the two non-vanishing elements of the regional MT tensor will also be equal. This implies that either the regional host structure is 1-D, or that the (distorted) measurement has been made at a location in a 2-D region where the regional E-polarization and

B-polarization (impedance) phases happen to be the same even though the two apparent resistivities are different. In other words, it is impossible to determine from a single measurement of a 3-D MT tensor whose elements are all in phase whether it represents data subjected to (real) galvanic distortion by a local anomaly in a 1-D or in a 2-D host region; and if it is the latter, then the direction of strike is indeterminate. The one exception is when $s_{41}=0$, because, provided that $\zeta_4\neq 0$, the conditions then degenerate to those for a simple 2-D model with no distortion, for which the angle of strike is given by eq. (25). (If $\zeta_4=0$ with $\zeta_1\neq 0$, it follows that there is an angle θ' given by $\tan 2\theta'=\xi_2/\xi_3=\eta_2/\eta_3$ for which M' becomes diagonal, indicative of an extreme distortion of a 1-D or 2-D regional MT tensor with the distortion angles ϕ_1 and ϕ_2 both equal to $\pm\pi/2$.)

We now concentrate on conditions (44) above. Suppose first that for the three invariants expressed in eq. (28) $s_{41}\neq 0$ and $d_{41}=d_{23}=0$. Setting $d_{41}=d_{23}=0$ in the identity (30), substituting in (42) multiplied through by $(d_{12}-d_{34})$, and noting that its right-hand side then vanishes for the value of θ' given by (44), we obtain by comparison with (39) and (40)

$$-\frac{\mathscr{R}e\,\mathsf{M}'_{11}}{\mathscr{R}e\,\mathsf{M}'_{21}}=\frac{\mathscr{I}m\,\mathsf{M}'_{22}}{\mathscr{I}m\,\mathsf{M}'_{12}}=\frac{\mathscr{R}e\,\mathsf{M}'_{22}}{\mathscr{R}e\,\mathsf{M}'_{12}}=-\frac{\mathscr{I}m\,\mathsf{M}'_{11}}{\mathscr{I}m\,\mathsf{M}'_{21}}\,. \tag{46}$$

It may be deduced immediately from eqs (38) that $\phi_1=\phi_2=\phi$ (say), so that, in the language of Groom & Bailey (1989), the resulting distortion is simply a pure twist without shear. In the special case $g_1=g_2=g=1/h$, it follows that $\mathsf{D}=h\mathsf{R}_{\phi}$ or $\mathsf{A}=g\mathsf{R}_{-\phi}$, where R is the rotation matrix (3). Such a distortion represents a local rotation of the regional electric field through an angle $-\phi$ and its amplification by a factor g; it could be caused by nothing more than a misalignment of the electrodes during the field experiment (Cox *et al.* 1980; Bahr 1988).

Next, we assume $d_{41}\neq 0$. Unfortunately, the vanishing of d_{23} (or $\sin\psi$) alone does not appear to have a simple physical interpretation. The form of eqs (39) and (40) suggests that more useful information could be extracted from the invariant $d_{41}-d_{23}$. If $d_{41}\neq 0$, its vanishing implies $d_{23}=d_{41}$, while otherwise d_{41} and d_{23} must vanish together as assumed in the previous case. Moreover, we deduce from eqs (28) that

$$d_{41}-d_{23}=\sin(\beta-\alpha)-\sin\gamma\sin\delta\sin\psi\,, \tag{47}$$

which shows how the invariant $d_{41}-d_{23}$ is related to $\sin\psi$. It is also closely associated with the 'phase-sensitive skew' of Bahr (1988, 1991), which in our notation is defined as $(I_1I_2|d_{41}-d_{23}|)^{1/2}/|\zeta_4|$.

Let us suppose, therefore, that $d_{23}=d_{41}\neq 0$. The MT tensor can always be decomposed into a 2-D form with the angles ϕ_1 and ϕ_2 in the distortion matrix given by (38) and the angle of the 2-D regional strike given by (44). There is, however, a way of normalizing this invariant that leads to a simpler interpretation of its meaning. Let θ_1 and θ_2 be the angles, whose existence is assumed for now, through which the axes must be rotated in order to satisfy the first and second of eqs (35) respectively. Then the *difference* between these two angles must be the same whatever the original frame of reference, that is, the angle $\theta_1-\theta_2$ is an obvious invariant. In a regional 3-D structure the two eqs (35) cannot be satisfied simultaneously, so that θ_1 and θ_2 are different; but we have seen already that if there is only localized 3-D distortion in an otherwise 2-D region, then $\theta_1=\theta_2=\theta'$. Thus $\theta_1-\theta_2$ is an invariant that vanishes when small-scale galvanic distortion occurs in a 2-D host region, but is otherwise non-vanishing in a general 3-D region. Now the first of eqs (35) is equivalent to the left-hand side of (39) vanishing, and the resulting equation for θ_1 can be expressed in the form

$$Q\sin(2\theta_1-2\theta')-d_{41}+d_{23}=0\,, \tag{48}$$

where Q is defined in (29) and θ' in (44). Similarly, the second of eqs (35) is satisfied when the left-hand side of (40) vanishes, so that θ_2 is given by

$$Q\sin(2\theta'-2\theta_2)-d_{41}+d_{23}=0\,. \tag{49}$$

An immediate consequence of these equations is the necessary and sufficient condition $|d_{41}-d_{23}|\leq|Q|\neq 0$ for the angles θ_1 and θ_2 to exist, and it follows that when this condition is satisfied $\theta'=(\theta_1+\theta_2)/2$, that is, θ' defines the bisector of the angle $\theta_1-\theta_2$. Substitution for θ' in either (48) or (49) immediately yields the solution

$$\sin(\theta_1-\theta_2)=(d_{41}-d_{23})/Q\,. \tag{50}$$

When $d_{41}=d_{23}$, we obtain $\theta_1=\theta_2=\theta'$ as required for galvanic distortion in a 2-D region.

It is now clear that the remaining three independent invariants are most usefully defined as follows:

$$I_5=\sin(\beta+\alpha)=s_{41}\,,\quad I_6=\sin(\beta-\alpha)=d_{41} \tag{51}$$

and

$$I_7=\sin(\theta_1-\theta_2)=\frac{d_{41}-d_{23}}{[(d_{12}-d_{34})^2+(d_{13}+d_{24})^2]^{1/2}}\,. \tag{52}$$

Note that their trigonometric representations show that the invariants I_3, I_4, $|I_5|$, $|I_6|$ and $|I_7|$ are all bounded above and below by 1 and 0 respectively. We recall also that when $I_6=0$ and $Q=0$, the numerator of I_7 also vanishes and I_7 becomes indeterminate.

4.4 Discussion

When $I_j=0$ ($j=3, 4, 5, 6$), the model is 1-D. It follows immediately from these conditions that $Q=0$ so that I_7 is undefined for a 1-D structure.

If $I_j\neq 0$ ($j=3$ or 4), $I_5=I_6=0$ with $\zeta_4\neq 0$, and either $I_7=0$ or, if it is undefined, $Q=0$, then the model is 2-D with the angle of strike given by (25). (In the latter case the phases in E-polarization and B-polarization are equal.) In the special case $\zeta_4=0$, there is local distortion in a 1-D or 2-D region such that M' assumes a diagonal form in the frame defined by the angle θ' satisfying $\tan 2\theta'=\xi_2/\xi_3=\eta_2/\eta_3$.

If $I_j\neq 0$ ($j=3$ or 4, 5), $I_6=0$, and I_7 is undefined with $Q=0$, then $d_{12}=d_{13}=d_{23}=d_{24}=d_{34}=d_{41}=0$ and the arguments or phases of all four elements of the MT tensor are equal, thereby indicating small-scale galvanic distortion in a 1-D region or at a point in a 2-D region where the phases are the same for both E-polarization and B-polarization. Bahr (1991) has devised an invariant 'phase difference measure', defined in the notation of this paper by $\mu=[I_1I_2(|d_{41}|+|d_{23}|)]^{1/2}/|\zeta_4|$, which plays a similar role to Q in that it reduces to zero when all the tensor elements have the same phases (arguments). It does not distinguish, however, between equal phases and a pure twist of the field because it obviously vanishes when $I_6=I_7=0$ as well; Q cannot vanish when $I_7=0$.

The conditions $I_j \neq 0$ ($j = 3$ or 4, 5), $I_6 = I_7 = 0$, which imply $d_{41} = d_{23} = 0$ or $\beta = \alpha$ and $\psi = 0$, indicate galvanic distortion representing a pure twist, without shear, of the local electric field in a 2-D region. The direction of strike in the regional structure is given by (44).

The conditions $I_6 \neq 0$, $I_7 = 0$ indicate that $\theta_1 = \theta_2$ so that eqs (35) are satisfied, and therefore the MT tensor can be decomposed by rotation and real distortion into a regional 2-D tensor. The angle of rotation θ' is given by eq. (44), which agrees with the result originally obtained by Bahr (1988, eq. 19). [It is worth pointing out that when $I_5 = I_6 = I_7 = 0$, so that $\xi_1 = \eta_1 = 0$, $d_{23} = 0$, and the structure is purely 2-D with no galvanic distortion—the case described in the second paragraph of this section—(44) reduces to $\tan 2\theta' = -d_{34}/d_{24}$, which readily simplifies to the required expression (25).] To perform the decomposition we note that the inverse of $\bar{\mathsf{M}} = \mathsf{D}\mathsf{M}'$ can be written, with the aid of (31), as

$$\mathsf{M}' = \mathsf{A}\bar{\mathsf{M}}' \equiv \begin{pmatrix} \cos\phi_1 & -\sin\phi_2 \\ \sin\phi_1 & \cos\phi_2 \end{pmatrix} \begin{pmatrix} 0 & g_1\bar{\mathsf{M}}'_{12} \\ g_2\bar{\mathsf{M}}'_{21} & 0 \end{pmatrix}. \qquad (53)$$

It represents four complex (eight real) equations in the four real and two complex unknowns g_1, g_2, ϕ_1, ϕ_2, $\bar{\mathsf{M}}'_{12}$, $\bar{\mathsf{M}}'_{21}$. As Smith (1995) has pointed out, however, the parameters g_1 and g_2 are revealed in (53) as nothing more than frequency-independent scaling factors of the elements of $\bar{\mathsf{M}}'$. Thus it is the 'static shifts' $g_1\bar{\mathsf{M}}'_{12}$ and $g_2\bar{\mathsf{M}}'_{21}$ of the regional tensor components that become the actual unknown quantities along with ϕ_1 and ϕ_2, rather than the original unscaled values. The number of real unknowns is therefore reduced to six, and g_1 and g_2 become indeterminate. Two underlying assumptions in Smith's analysis were (i) that the regional structure is indeed 2-D, and (ii) that the measured values of the MT tensor are provided in the frame of reference aligned along the regional strike, thereby implying $\theta' = 0$. Thus Smith assumed that the values of M'_{ij} rather than M_{ij} are given, and he regarded (53) as an overdetermined system of eight real equations in six real (two complex plus two real) unknowns. Our approach is slightly different. We require the condition $I_7 = 0$ to be satisfied with the angle θ' given by eq. (44) before proceeding with the decomposition. Thus the knowledge of θ' allows one to determine M' from M by rotation, and the fact that $I_7 = 0$ means that eqs (38) are effectively prescribed, thereby providing the solutions for ϕ_1 and ϕ_2 and rendering four of the eight equations (53) redundant. The remaining four equations are just sufficient in number to determine the modified complex elements $g_1\bar{\mathsf{M}}'_{12}$ and $g_2\bar{\mathsf{M}}'_{21}$ of the regional tensor, which can be expressed in the form

$$g_1 \mathscr{R}e\, \bar{\mathsf{M}}'_{12} = \mathrm{sgn}\,(\mathscr{R}e\, \mathsf{M}'_{12})[(\mathscr{R}e\, \mathsf{M}'_{12})^2 + (\mathscr{R}e\, \mathsf{M}'_{22})^2]^{1/2}, \qquad (54)$$

$$g_1 \mathscr{I}m\, \bar{\mathsf{M}}'_{12} = \mathrm{sgn}\,(\mathscr{I}m\, \mathsf{M}'_{12})[(\mathscr{I}m\, \mathsf{M}'_{12})^2 + (\mathscr{I}m\, \mathsf{M}'_{22})^2]^{1/2}, \qquad (55)$$

$$g_2 \mathscr{R}e\, \bar{\mathsf{M}}'_{21} = \mathrm{sgn}\,(\mathscr{R}e\, \mathsf{M}'_{21})[(\mathscr{R}e\, \mathsf{M}'_{11})^2 + (\mathscr{R}e\, \mathsf{M}'_{21})^2]^{1/2}, \qquad (56)$$

$$g_2 \mathscr{I}m\, \bar{\mathsf{M}}'_{21} = \mathrm{sgn}\,(\mathscr{I}m\, \mathsf{M}'_{21})[(\mathscr{I}m\, \mathsf{M}'_{11})^2 + (\mathscr{I}m\, \mathsf{M}'_{21})^2]^{1/2}, \qquad (57)$$

where, as usual, sgn x is defined to be $+1$ if $x > 0$ and -1 if $x < 0$.

Finally, if $I_7 \neq 0$ [including the case when $|d_{41} - d_{23}| > |Q| \neq 0$, which implies there are no rotated frames in which eqs (35) are satisfied], then the structure should be assumed to be regionally 3-D.

The properties and geometrical representations of the seven invariants I_1 to I_7 have been summarized for easy reference in Table 1.

With real data that includes random instrumental noise (often assumed to be Gaussian) as well as 'geological noise' arising because actual geoelectric structures never conform to the idealized models considered in the preceding theory, we cannot expect invariants to vanish precisely. Even the responses of purely synthetic configurations generated by 3-D forward modelling programs will necessarily be contaminated with numerical noise caused by round-off and the approximations introduced by discretization. Given that $0 \leq |I_j| \leq 1$, ($j = 3, 4, 5, 6, 7$), as noted at the end of Section 4.3, it is suggested that physical interpretations of the structure based on the vanishing of one or more invariants are approximately realized if the absolute values of the relevant invariants assume values of 0.1 or less, or equivalently, that the angles whose sines the invariants represent are less than about 5.7°. (To test for the special case $\zeta_4 = 0$, we would require $\xi_4/I_1 \equiv \cos\alpha < 0.1$ and $\eta_4/I_2 \equiv \cos\beta < 0.1$.) This is a subjective decision, but as shown later, it appears to be satisfactory when the data are subject to 2 per cent noise, and it is consistent with the practice introduced by Bahr (1988, 1991), who set his 'phase sensitive skew' and 'phase difference measure' to zero if they were less than 0.1.

5 A SYNTHETIC EXAMPLE

The synthetic model of the earth used to investigate the behaviour of the seven invariants I_1 to I_7 is depicted in Fig. 3. It consists of a conductive cubic anomaly, of resistivity 0.5 Ω m and dimensions 1 km, embedded at the surface of an otherwise 2-D structure. The centre of the cube is located 10.5 km from a vertical fault that divides the region hosting the anomaly (a slab of resistivity 10 Ω m and thickness 5 km) from a uniform quarter-space of resistivity 1 Ω m. Beneath the slab there is a 100 Ω m resistive layer 45 km thick, which in turn is underlain by a uniform region of resistivity 1 Ω m. The direction of strike of the fault is taken to be inclined at an angle of 40° to the north, as shown in Fig. 3. The MT tensor is calculated in the (x, y) coordinate frame defined by the directions of north and east, while the rotated x' and y' axes in the rotated frame are aligned respectively along and perpendicular to the fault line on the surface of the model; the z-axis is directed vertically downwards. The origin O is positioned so that the cubic anomaly is symmetrically placed with respect to the y'-axis and occupies the region $-0.5 < x' < 0.5$, $-11 < y' < -10$, $0 < z < 1$ in kilometre units.

Numerical calculations were performed for three separate periods of the inducing field, 1 s, 100 s and 1000 s, using a 3-D modelling program (Weaver *et al.* 1999) in which integral boundary conditions are employed at the surface and the 3-D resistivity model is permitted to approach 2-D limiting structures on its boundaries, as in Fig. 3. In practice, the E-polarization and B-polarization electric and magnetic field components were calculated in the (x', y') coordinate frame and then rotated through $-40°$ for computation of the MT tensor. We first examine the invariants of the MT tensors calculated directly from the computer-generated solutions for one or more periods at four particular sites that are chosen to

Table 1. Summary of the properties of the seven independent invariants I_1 to I_7 and the dependent invariant Q. S–M (column 3) refers to Szarka & Menvielle (1997).

Invariant	Mohr circle diagram	Related S–M invariant	Physical interpretation
$I_1=(\xi_4^2+\xi_1^2)^{1/2}$ $I_2=(\eta_4^2+\eta_1^2)^{1/2}$	$OC=I_1$ $OD=I_2$	ξ_4 η_4	If $I_3=I_4=I_5=I_6=0$, a 1-D structure of apparent resistivity $\mu_0(I_1^2+I_2^2)/\omega$ and its associated phase $\arctan(I_2/I_1)$ is implied.
$I_3=(\xi_2^2+\xi_3^2)^{1/2}/I_1$ $I_4=(\eta_2^2+\eta_3^2)^{1/2}/I_2$	$\sin\gamma$ $\sin\delta$	$\det(\mathscr{R}e\,\mathsf{M})$ $\det(\mathscr{I}m\,\mathsf{M})$	If $I_3\neq0$ or $I_4\neq0$, $I_5=I_6=0$, ($\zeta_4\neq0$) and either $I_7=0$ or $Q=0$, conditions for a 2-D structure with strike angle θ' satisfying (25) are satisfied. (In the special case $\zeta_4=0$, distortion in a 1-D or 2-D region occurs as discussed in the main text.)
$I_5=s_{41}=\dfrac{\xi_4\eta_1+\xi_1\eta_4}{I_1I_2}$	$\sin(\beta+\alpha)$	ξ_1, η_1	If $I_3\neq0$ or $I_4\neq0$, $I_5\neq0$ and $I_6=I_7=0$, then the local electric field has undergone a pure twist (misalignment of the electrodes?) in a 2-D region with strike angle θ' given by (44). If I_7 is indeterminate with $Q=0$, then there is in-phase, small-scale distortion in a 1-D region, or in a 2-D region where the E- and B-polarization (impedance) phases are equal. In the latter case, the strike angle is not recoverable.
$I_6=d_{41}=\dfrac{\xi_4\eta_1-\xi_1\eta_4}{I_1I_2}$	$\sin(\beta-\alpha)$	ξ_1, η_1	If $I_6\neq0$, $I_7=0$, conditions for in-phase small-scale distortion in a 2-D region with strike angle θ' given by (44) are satisfied.
$I_7=(d_{41}-d_{23})/Q$	$[\sin(\beta-\alpha)-\sin\gamma\sin\delta\sin\psi]/Q$ $=\sin(\theta_1-\theta_2)$	$\mathscr{I}m(\det\mathsf{M})$	If I_7 is non-negligible, a regional 3-D structure is indicated. θ_1 and θ_2 are those angles through which the axes must be rotated to make the elements in the first and second columns of M, respectively, have equal phases.
$Q=[(d_{12}-d_{34})^2$ $+(d_{13}+d_{24})^2]^{1/2}$	$\sin^2\gamma+\sin^2\delta$ $-2\sin\gamma\sin\delta\cos(\beta-\alpha-\psi)$		A supplementary dependent invariant whose vanishing implies that the tensor elements have equal arguments, that $I_3=I_4$ and $d_{41}=d_{23}$, i.e. that I_7 is undefined.

illustrate the properties discussed above. Subsequently we consider more realistic numerical data that has been contaminated with 2 per cent Gaussian noise.

5.1 Noise-free results

The four chosen sites for which the computations were made are defined as follows:

SITE 1: $x'=140$, $y'=-126$,

SITE 2: $x'=140$, $y'=-11.125$,

SITE 3: $x'=0.625$, $y'=-11.125$,

SITE 4: $x'=0.625$, $y'=-10.13$.

All the numerical results are quoted to three significant figures.

(a) SITE 1: $T=100$ s.

$$\mathsf{M}=\begin{pmatrix}-2.28-i\,2.94 & 1070+i\,576\\ -1070-i\,575 & 2.28+i\,2.94\end{pmatrix},$$

$I_1=1.07$ km s^{-1}, $I_2=0.576$ km s^{-1},

$I_3=0.002$, $I_4=0.005$,

$I_5=0$, $I_6=0$,

$I_7=0$, $Q=0.003$.

Since the site is many skin depths removed from both the anomaly and the fault line, the MT tensor clearly exhibits properties associated with a 1-D region. Note that $Q\approx0$, as expected, so that I_7 is undefined and its computed value meaningless. With $\mu_0=4\pi\times10^{-7}$ H m^{-1}, the apparent resistivity is given by $T(I_1^2+I_2^2)/5=29.5$ Ω m and the phase angle is $\arctan(I_2/I_1)=28.7°$. (The correct values for the 1-D structure at $y=-\infty$ are 29.1 Ω m and 29.0°.)

(b) SITE 2: $T=1000$ s.

$$\mathsf{M}=\begin{pmatrix}39.7+i\,76.9 & 118+i\,240\\ -132-i\,267 & -39.7-i\,76.9\end{pmatrix},$$

$I_1=0.125$ km s^{-1}, $I_2=0.254$ km s^{-1},

$I_3=0.324$, $I_4=0.308$,

$I_5=0$, $I_6=0$,

$I_7=0.005$, $Q=0.015$.

This site is far from the anomaly but less than a skin depth from the 2-D fault. The invariants I_1, I_2, I_3 and I_4 are non-negligible but $I_5=I_6=0$ and $Q\approx0$, indicating a 2-D response with equal phases in E-polarization and B-polarization (the computed value of I_7 is again meaningless). In fact, if the negative signs in the second row are ignored (because they only have the effect of subtracting 180°), the arguments of the elements of M are calculated to be 62.7°, 63.8°, 63.7° and 62.7°,

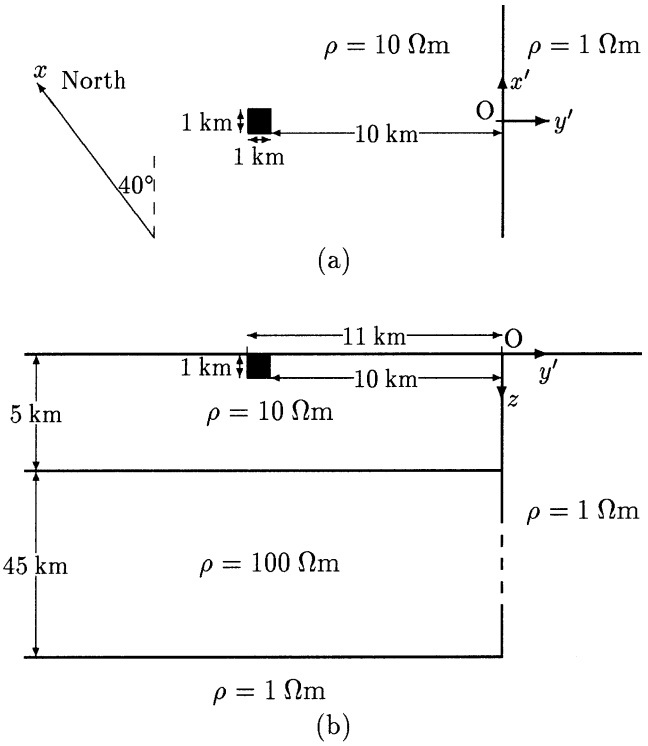

Figure 3. (a) The surface plane $z=0$ viewed from above and (b) vertical cross-section in the plane $x'=0$ of the model chosen for numerical investigation. The small anomaly is a 1 km^3 cubic block, depicted by the black region in the diagram, whose centre is 10.5 km from a 2-D fault dividing a two-layered slab 50 km thick from a conductive region of resistivity 1 Ω m that also underlies the slab. The anomalous block has a resistivity of 0.5 Ω m. The x'-axis representing the fault line is inclined at an angle of 40° to the x-axis defining the direction of north, as shown.

that is, they are indeed all approximately equal. The angle of strike calculated from eq. (25) is found to be exactly 40°. Note that $I_3 \approx I_4$ as predicted in Section 4.3 when $Q=0$.

(c) SITE 2: $T=100$ s.

$$\mathsf{M}=\begin{pmatrix} 228-i54.2 & 812+i619 \\ -892-i600 & -228+i54.2 \end{pmatrix},$$

$I_1=0.852$ km s^{-1}, $I_2=0.609$ km s^{-1},

$I_3=0.271$, $I_4=0.090$,

$I_5=0$, $I_6=0$,

$I_7=0$, $Q=0.362$.

At this shorter period the site is even further removed (in skin depths) from the anomaly but still near enough to the fault to register a 2-D response, although the out-of-phase response is virtually 1-D since I_4 is on the borderline of being negligible. The angle of strike was again found to be exactly 40°. An important difference from the previous case is that Q is non-negligible so that the computed value $I_7=0$ is now meaningful. The site is therefore in a 2-D region where the phases are different in E-polarization and B-polarization; in fact, the arguments of the elements of M (with negative signs in the second row again extracted) are found to be −13.4°, 37.3°, 33.9° and −13.4°, which are certainly no longer nearly equal. For later reference, we note that the non-vanishing components of M′ in the rotated frame aligned with the strike direction of the fault are $\mathsf{M}'_{12}=621+i664$ and $\mathsf{M}'_{21}=-1080-i554$.

(d) SITE 3: $T=1000$ s.

$$\mathsf{M}=\begin{pmatrix} 68.9+i131 & 174+i353 \\ -86.5-i178 & -34.7-i64.9 \end{pmatrix},$$

$I_1=0.131$ km s^{-1}, $I_2=0.268$ km s^{-1},

$I_3=0.516$, $I_4=0.490$,

$I_5=0.252$, $I_6=-0.007$,

$I_7=0.012$, $Q=0.027$.

Here only I_6 and Q are negligible (the latter again implying that I_7 is undefined and $I_3 \approx I_4$). Thus real distortion in either a 1-D region or a 2-D region where the E-polarization and B-polarization phases are the same is indicated. We have already seen in example (b) above that at this period and lateral displacement from the fault, the undistorted fields are indeed 2-D and in phase. The angle of strike cannot be recovered under these circumstances.

(e) SITE 2: $T=100$ s with a 10° twist of the electric field.

A 10° misalignment of the electrodes is simulated by rotating the calculated electric field components by only −30° rather than the −40° through which the magnetic field components are rotated after they have been calculated in the frame defined by the strike of the fault. The matrix and invariants of the resulting MT tensor are

$$\mathsf{M}=\begin{pmatrix} 69.2-i157 & 760+i619 \\ -918-i581 & -365-i54.1 \end{pmatrix},$$

$I_1=0.852$ km s^{-1}, $I_2=0.609$ km s^{-1},

$I_3=0.271$, $I_4=0.090$,

$I_5=-0.342$, $I_6=0$,

$I_7=0.001$, $Q=0.361$,

which are completely different from the corresponding figures for the untwisted field at the same site given in example (c). Here I_6 and I_7 are vanishingly small but Q is non-negligible, which indicates a pure twist of the electric field in a 2-D region. The angle of strike is given by eq. (44) as exactly 40° and when the axes are rotated by this angle into the frame defined by the strike, the matrix M′ of the MT tensor becomes

$$\mathsf{M}'=\begin{pmatrix} -188-i96.2 & 611+i654 \\ -1070-i546 & -108-i115 \end{pmatrix}.$$

The equations (46) should give the same angle of twist $-\phi$. In fact, we obtain the four values 9.97°, 9.99°, 10.0° and 9.97°, which to two significant figures are indeed all equal to the actual twist of 10°.

(f) SITE 3: $T=100$ s.

$$\mathsf{M}=\begin{pmatrix} 392-i39.9 & 1190+i863 \\ -588-i390 & -200-i4.24 \end{pmatrix},$$

$I_1=0.894$ km s^{-1}, $I_2=0.627$ km s^{-1},
$I_3=0.473$, $I_4=0.378$,
$I_5=0.072$, $I_6=-0.142$,
$I_7=-0.025$, $Q=0.308$.

Here I_6 is non-negligible while I_7 is negligible and defined (because Q is non-negligible), which points to small-scale, in-phase distortion in a regional 2-D setting. The angle of strike was recovered from eq. (44) as 42.2° and in the frame rotated through this angle M' is given by

$$\mathsf{M}'=\begin{pmatrix} 425+i211 & 623+i667 \\ -1150-i585 & -233-i256 \end{pmatrix}.$$

Thus, according to eqs (38),

$\phi_1=-20.5°$, $\phi_2=20.2°$

if the ratios of real parts are used, while the ratios of imaginary parts give

$\phi_1=-21.0°$, $\phi_2=19.9°$.

It would be appropriate to use the first two values when calculating the distortion matrix acting on $\mathscr{R}e\,\bar{\mathsf{M}}'$ and the second pair for the matrix distorting $\mathscr{I}m\,\bar{\mathsf{M}}'$. From eqs (54)–(57) we have

$g_1\bar{M}'_{12}=665+i714$, $g_2\bar{M}'_{21}=-1230-i622$.

Since we know from example (c) the true 2-D regional tensor at the given period and distance from the fault, it is possible to calculate g_1 and g_2 theoretically for this synthetic model even though they would be indeterminate with real data and no prior knowledge of the regional tensor. Dividing the equations above by the corresponding equations at the end of example (c), we obtain

$g_1=1.07+i0.002$, $g_2=1.14-i0.007$,

which are virtually real numbers, as they should be. Setting the imaginary parts to zero and using the values for ϕ_1 and ϕ_2 from above, we find from (31) that the distortion matrices A acting on the real and imaginary parts of $\bar{\mathsf{M}}'$ are

$$\begin{pmatrix} 1.01 & -0.391 \\ -0.375 & 1.06 \end{pmatrix} \text{ and } \begin{pmatrix} 1.00 & -0.385 \\ -0.384 & 1.07 \end{pmatrix}$$

respectively. Likewise, the corresponding inverse matrices $\mathsf{D}\equiv\mathsf{A}^{-1}$ are given by (32) as

$$\begin{pmatrix} 1.15 & 0.424 \\ 0.407 & 1.09 \end{pmatrix} \text{ and } \begin{pmatrix} 1.16 & 0.418 \\ 0.417 & 1.09 \end{pmatrix}.$$

When the last two 'undistorting' matrices act on the respective real and imaginary parts of M' given above and the resulting matrix is rotated back through the $-42.2°$ calculated from eq. (44), the matrix

$$\mathsf{M}=\begin{pmatrix} 232-i57.7 & 830+i613 \\ -875-i602 & -232+i57.6 \end{pmatrix}$$

is recovered, which is very close to the true 2-D matrix given by M in example (c).

(g) SITE 4: $T=1$ s.

$$\mathsf{M}=\begin{pmatrix} -3420-i1550 & 3800+i4220 \\ -6700-i5010 & 1750+i942 \end{pmatrix},$$

$I_1=5.32$ km s^{-1}, $I_2=4.62$ km s^{-1},
$I_3=0.557$, $I_4=0.283$,
$I_5=-0.222$, $I_6=0.092$,
$I_7=0.216$, $Q=0.278$.

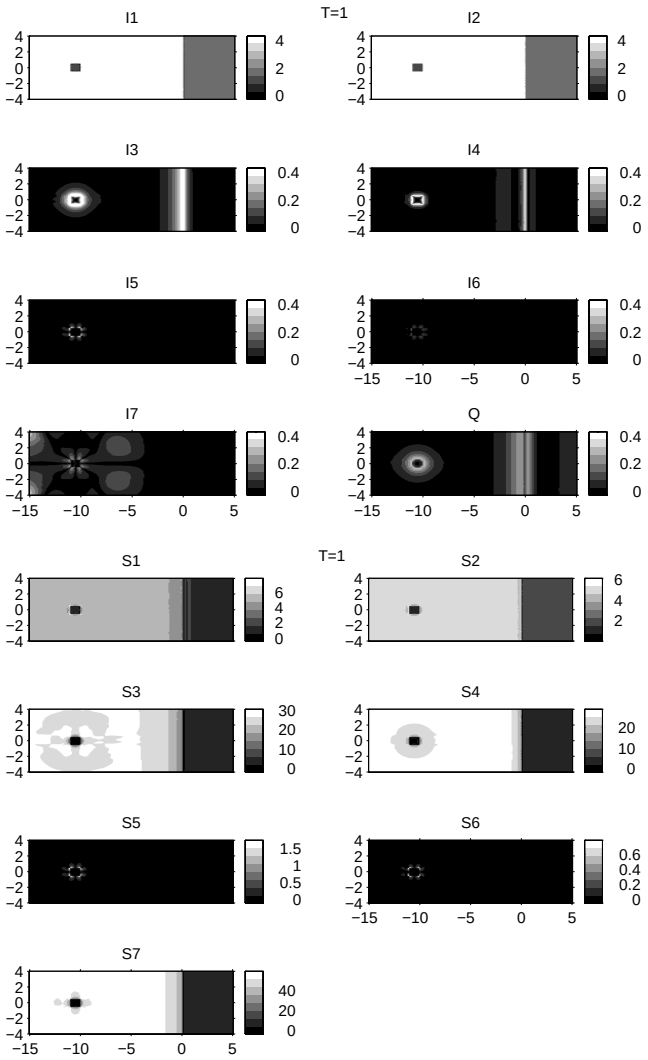

Figure 4. Grey-scale contour maps in the surface plane $z=0$ of the seven invariants and Q for a period of 1 s. From top to bottom the plots are of the invariants I_1 (left) and I_2 (right), I_3 and I_4, I_5 and I_6, I_7 and Q in the upper diagram; they are compared with the corresponding plots of the seven S–M invariants ξ_4 (left) and η_4 (right), det ($\mathscr{R}e\,\mathsf{M}$) and det ($\mathscr{I}m\,\mathsf{M}$), ξ_1 and η_1, and $\mathscr{I}m$ (det M) shown in the lower diagram. The vertical and horizontal scales give the coordinates x and y respectively in kilometres. The invariants I_1, I_2, ξ_4, η_4, ξ_1 and η_1 are expressed in units of km s^{-1}, and det ($\mathscr{R}e\,\mathsf{M}$), det ($\mathscr{I}m\,\mathsf{M}$) and $\mathscr{I}m$ (det M) in units of km^2 s^{-2}.

At this short period the skin depth in the cubic block is only 0.36 km, which means that its dimensions are equal to 2.8 skin depths. It can therefore no longer be considered as a small anomaly that merely distorts the electric currents induced in the regional structure. It acts at this period as a fully 3-D body in its own right; currents are induced in the block and their phases change significantly over its thickness. This is an example of induction in a 3-D body and, appropriately, I_7 is defined and non-negligible.

In Figs 4 and 5, the variation of the seven invariants and Q for the three periods 1, 100 and 1000 s over the entire surface plane is displayed in grey-scale diagrams and compared with the corresponding variation of the S–M invariants. These plots portray a revealing overview of the underlying structure. At the short 1 s period in Fig. 4, the 3-D cubic anomaly is seen in all the invariants. Away from the anomaly the response is generally that of a 1-D structure because all the invariants other than I_1 and I_2 are very small or, in the case of I_7, indeterminate in those regions where Q is small (dark). The light bands in I_3 and I_4 near $y=0$ indicate that the region of two-dimensionality is relatively narrow at this short period, and the edges of the anomaly show up as 2-D boundaries in the same plots. At the period of 100 s shown in the left-hand columns of Fig. 5, the anomaly virtually disappears in the plot of I_7 but is apparent in the plots of I_5 and I_6, thereby pointing to real distortion in a 2-D region as discussed in example (f) above. The wider region of two-dimensionality associated with the greater skin depth at this period is apparent in I_3 and I_4. Finally, for the 1000 s period in the right-hand columns of Fig. 5 the anomaly is invisible in I_6 and I_7 but is highlighted in I_5, while I_3 and I_4 indicate extensive regions of two-dimensionality associated with the fault along $y=0$. There is also a wide band of small Q values between the fault and the anomaly that maps the region where the 2-D E- and B-polarization phases are nearly the same and also where I_7 is undefined.

The variation of the S–M invariants depicted in the lower diagrams of Figs 4 and 5 are less easy to interpret physically. The anomaly is revealed in all of them for all three periods, as is the 2-D fault except in the plots of the invariants ξ_1 and η_1, which vanish in both 1-D and 2-D regions. Thus it seems difficult to ascertain what physical role the anomaly is

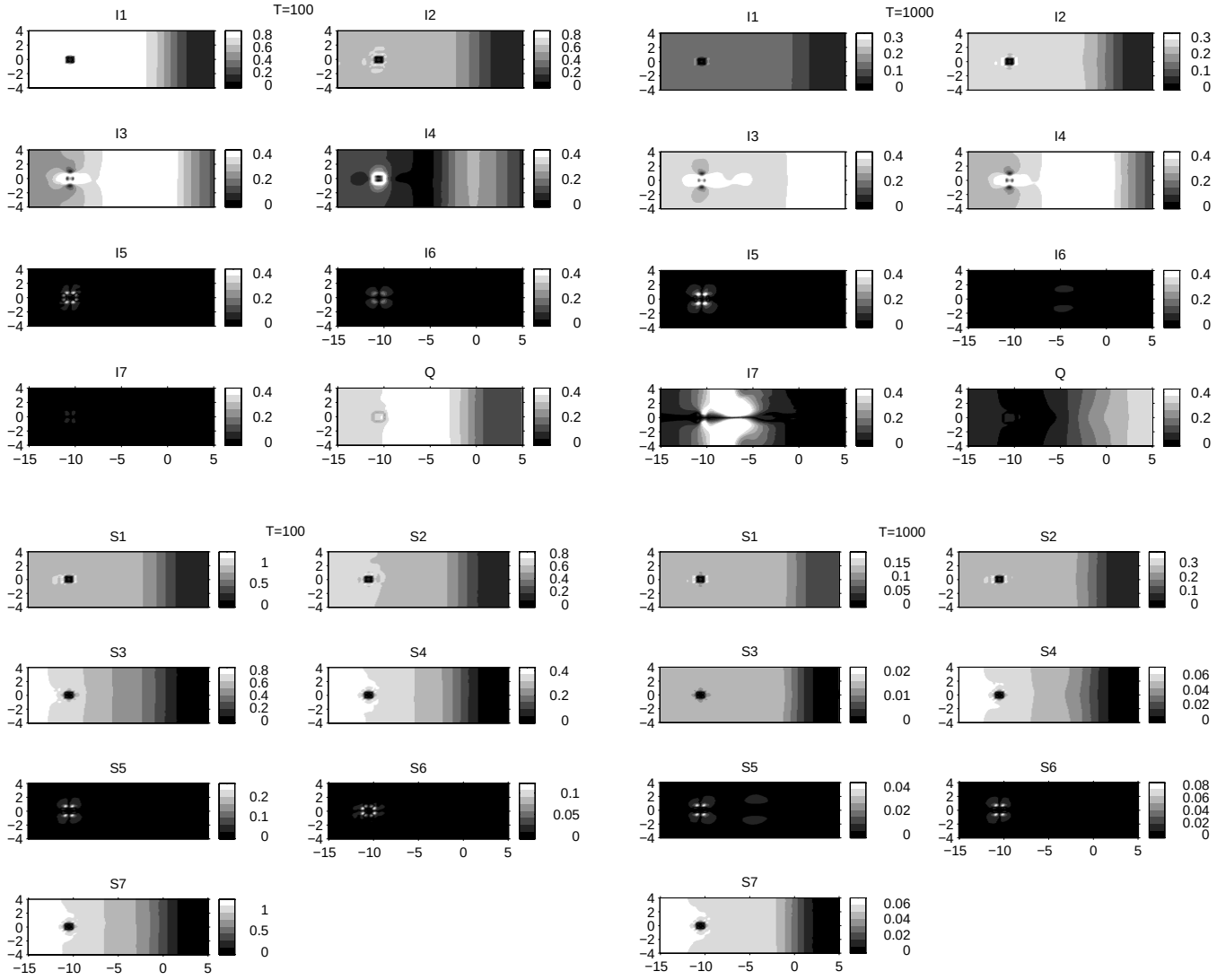

Figure 5. The same as Fig. 4 for periods of 100 s (left two columns) and 1000 s (right two columns).

playing from a mere perusal of the contour maps for the S–M invariants; it is those in the upper diagrams that reveal useful information in a systematic manner.

5.2 Calculations with noisy data

Real data are not single observations but samples of many measurements that are subject to instrumental and other noise. For a more realistic investigation, therefore, it is pertinent to examine the statistical behaviour of the invariants when the tensor elements have been treated with random noise. Jones & Groom (1993) undertook such a theoretical study in connection with the Groom–Bailey decomposition and showed that the shear parameter behaved robustly when Gaussian noise was added to the data, and that while the twist values were generally more widely scattered about their true value than the shear values, they were still relatively stable compared to the strike angle, whose behaviour could be fairly unstable. As a result, they have advocated fixing the twist and shear parameters to their average values before determining the angle of strike from noisy or real data.

Here we conduct a similar investigation of parameter stability in the presence of noise by simply calculating sample means and standard deviations of all seven invariants I_j, the dependent invariant Q and the strike angle θ'. First, the calculations of the previous section were repeated for noisy data formed by adding random Gaussian noise with a standard deviation of $(I_1^2+I_2^2)^{1/2}/50$ to the elements of the MT tensor, that is, 2 per cent Gaussian noise using the central impedances (divided by μ_0) as a representative value of the tensor. The process was repeated many times, so that random samples of various sizes could be selected. For the results presented here we chose a sample size of 100.

In Figs 6 and 7 we have plotted the values of the invariants I_j ($j=1, 2, \ldots, 7$), the dependent invariant Q and the strike angle θ' for 100 realizations of the noisy data calculated for the

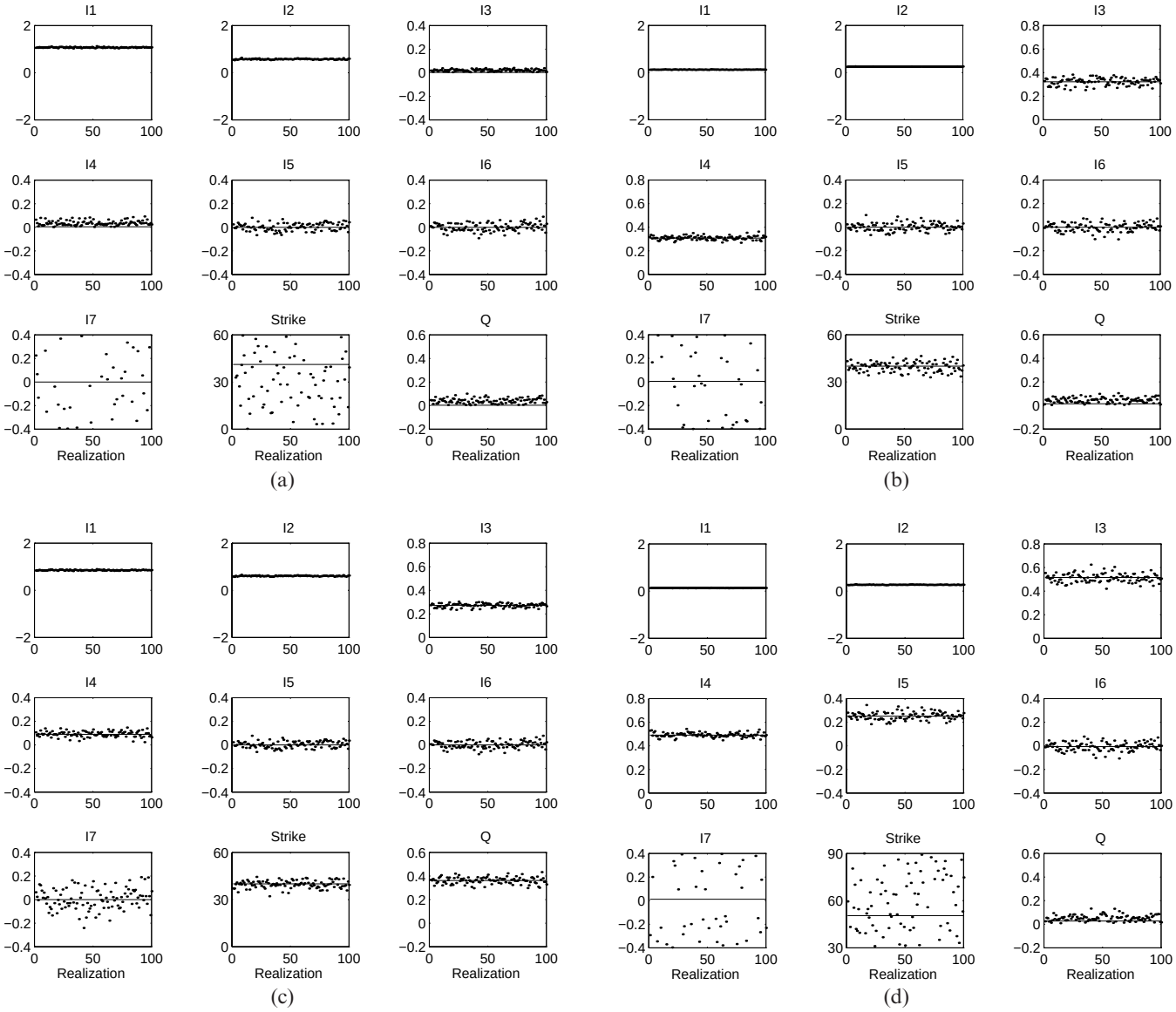

Figure 6. Plots of 100 realizations of the independent invariants I_j ($j=1, 2, \ldots, 7$), the dependent invariant Q, and the strike angle θ' for events (a) to (d) listed in Section 5.1 when Gaussian noise is added to the tensor elements. The solid lines represent the true values calculated from the original (noise-free) tensor. Note that I_7 is undefined when $Q \approx 0$, examples (a), (b) and (d), while the strike angle is indeterminate in (a) and (d).

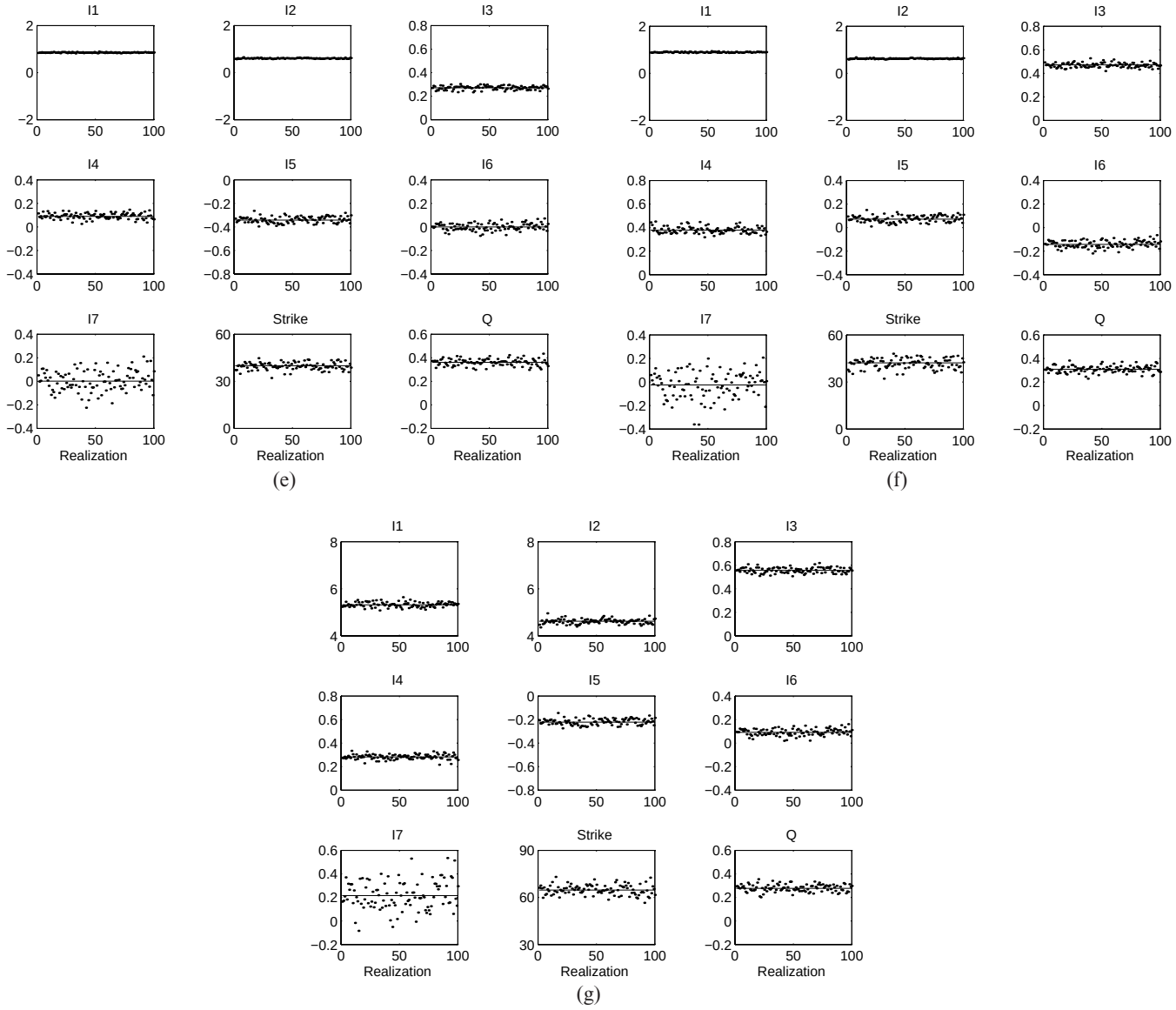

Figure 7. As in Fig. 6 for the events (e) to (g) listed in Section 5.1. Note that the strike angle cannot be determined in case (g) where $I_7 \approx 0$.

examples (a) to (g) considered in Section 5.1. They are shown as points scattered about the 'true' (noise-free) values indicated by the solid line. All calculations are shown, even though with our prior knowledge of the model it is known that some of the parameters will be highly unstable, i.e. theoretically indeterminate. The statistics of the calculations in the form of means and standard deviations are tabulated alongside the calculated true values in Table 2.

It is apparent at once from a quick perusal of the figures and accompanying table that I_7 is widely scattered in examples (a), (b) and (d), with large standard deviations, and its indeterminacy is confirmed by the clustering of Q near zero with its mean at least 1.5 standard deviations less than 0.1, which is the upper limit of our measure of 'negligible'. In all the other examples the mean of Q stays well above this value so that the associated values of I_7 are meaningful. Further examination of these special cases when $Q \approx 0$ show that in (a) invariants I_3 to I_6 all have means close to zero at least three standard deviations less than 0.1 so that the conditions for a 1-D structure are clearly fulfilled. The angle θ' is, of course, undefined in a 1-D region, which accounts for its scatter in Fig. 6 and large standard deviation in Table 2. In (b) I_3 and I_4 have small standard deviations but their means are well above 0.1, while I_5 and I_6 are still clustered about zero, with standard deviations well inside the negligible range; the structure is therefore 2-D with similar phases in E- and B-polarization, and the strike angle θ' defined by (25) is seen to be $40^\circ \pm 3^\circ$, the error range being defined by the standard deviation. Finally, in (d) the mean of I_5 is no longer small, distortion in either a 1-D region or in a 2-D region with similar phases in E- and B-polarization is indicated, and the large standard deviation shows that any calculated θ' is unreliable, as expected.

For the remaining cases when $Q \not\approx 0$, it is clear that the values of I_7 are more widely scattered than those of the other six invariants (which appear to be quite robust in their behaviour), with standard deviations typically about 0.1, that is, at the limit of our range of tolerance. Nevertheless, the mean values of I_7 are close to the noise-free values and in particular the

Table 2. True (noise-free) values compared with the means and standard deviations of a random sample of 100 values of the seven independent invariants for the events (a) to (g) listed in Section 5.1, calculated with 2 per cent Gaussian noise added to the elements of the MT tensor. Where I_7 and θ' are known to be indeterminate (because $Q \approx 0$), the true value entries are left blank. Note that the calculated noise-free value of θ' in (f) contains sufficient numerical noise that its 'true' value is given as 42.2° rather than the known value of 40°.

	True value	Mean value	Standard deviation
I_1	1.07	1.07	0.018
I_2	0.576	0.574	0.018
I_3	0.002	0.021	0.009
I_4	0.005	0.037	0.021
I_5	0	0.004	0.032
I_6	0	0.003	0.034
I_7		0.070	1.838
Q	0.003	0.041	0.022
θ'		45.1°	26.3°
		(a)	
I_1	0.131	0.132	0.004
I_2	0.268	0.267	0.004
I_3	0.516	0.512	0.037
I_4	0.491	0.493	0.019
I_5	0.252	0.254	0.033
I_6	−0.007	−0.005	0.037
I_7		−0.016	0.949
Q	0.027	0.053	0.026
θ'		48.6°	24.9°
		(d)	

	True value	Mean value	Standard deviation
I_1	0.125	0.126	0.004
I_2	0.254	0.253	0.004
I_3	0.323	0.323	0.031
I_4	0.308	0.310	0.017
I_5	0	0.003	0.034
I_6	0	0.001	0.037
I_7		0.169	1.39
Q	0.015	0.047	0.022
θ'	40.0°	39.6°	3.06°
		(b)	
I_1	0.852	0.854	0.016
I_2	0.609	0.608	0
I_3	0.271	0.272	0.016
I_4	0.090	0.093	0.025
I_5	−0.342	−0.338	0.027
I_6	0	0.002	0.030
I_7	0.001	0.006	0.087
Q	0.361	0.361	0.029
θ'	40.0°	39.7°	2.34°
		(e)	
I_1	5.32	5.33	0.107
I_2	4.62	4.62	0.105
I_3	0.557	0.558	0.024
I_4	0.283	0.283	0.022
I_5	−0.222	−0.218	0.026
I_6	0.092	0.093	0.029
I_7	0.216	0.220	0.122
Q	0.278	0.281	0.031
θ'		64.8°	3.20°
		(g)	

	True value	Mean value	Standard deviation
I_1	0.852	0.854	0.016
I_2	0.609	0.609	0.016
I_3	0.272	0.272	0.017
I_4	0.090	0.093	0.025
I_5	0	0.004	0.028
I_6	0	0.002	0.031
I_7	0	0.007	0.089
Q	0.362	0.362	0.029
θ'	40.0°	39.7°	2.38°
		(c)	
I_1	0.894	0.897	0.016
I_2	0.627	0.626	0.016
I_3	0.472	0.470	0.020
I_4	0.378	0.381	0.029
I_5	0.072	0.076	0.028
I_6	−0.142	−0.140	0.031
I_7	−0.025	−0.025	0.112
Q	0.308	0.309	0.030
θ'	42.2°	41.7°	3.23°
		(f)	

distinction between a negligible I_7, examples (c), (e) and (f), and a non-vanishing value indicating a full 3-D induction rather than galvanic distortion, example (g), is quite clear. The strike angles determined from (25) for (c) and (44) for (e) and (f) are also less tightly constrained, but in cases (c) and (e) they give accurate mean values with standard deviations of about 2.3° while in (f) the mean value is actually about 0.5° more correct than the noise-free 'true' value, but the standard deviation is just over 3°. The results for I_7 and θ' in (f) have also been displayed in Fig. 8 as histograms showing the number of realizations in intervals of 0.05 for I_7 and 1° for θ'. Although the spread in I_7 is at the limit of acceptability, the distribution of its sample values is well behaved. Likewise, the clustering of the values of θ' around its mean value resembles a slightly biased normal distribution and shows none of the erratic behaviour of strike angle calculations that has sometimes been observed.

6 CONCLUDING REMARKS

The primary intent of this paper was to devise an improved set of seven independent invariants of the MT tensor and to seek, in a systematic manner, simple physical interpretations of their vanishing in successive order, particularly with a view to identifying possible 3-D galvanic distortions in a regionally 2-D structure. All the proposed invariants can be identified geometrically on a Mohr circle diagram, and all except the first two (which define the fundamental 'core' of the tensor) have been expressed as the sine of an easily identifiable angle. In the course of the investigation, there emerged an eighth (dependent) invariant that plays an important role in identifying those special circumstances under which the direction of the regional 2-D strike becomes indeterminate and also when the data are undistorted but the (impedance) phases are the same in both E- and B-polarizations. The theoretical properties and physical interpretations of the invariants have been confirmed with the aid of 3-D calculations based on a simple synthetic model that, for different periods, includes all the various configurations of interest. An elementary analysis of the behaviour of the invariants when 2 per cent Gaussian noise was added to the tensor showed that the first six invariants appeared quite robust and that the seventh invariant was able to discriminate between full 3-D induction and small-scale 3-D galvanic distortion in an otherwise 2-D regional structure, even though it was less tightly constrained than the others. The corresponding angle of strike was also less robust statistically but it was determined, for this level of noise, with mean values of very acceptable accuracy and standard

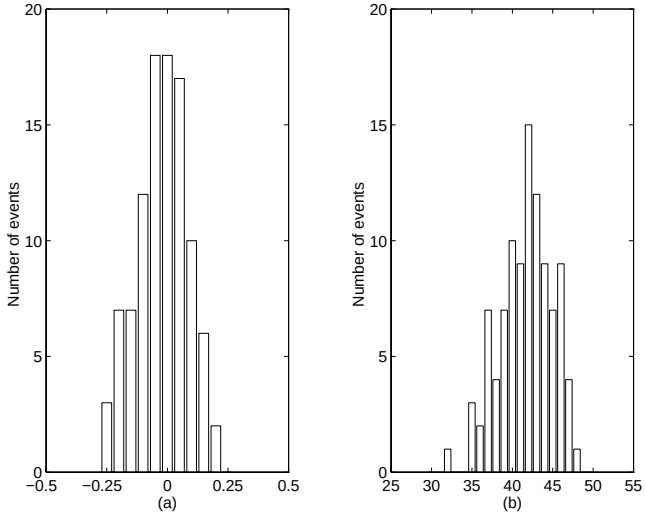

Figure 8. Histograms of (a) I_7 and (b) strike angle θ' in degrees, for a sample of 100 realizations of the response in case (f) calculated when 2 per cent noise is added to the tensor elements.

deviations ranging from 2.3° to 3.2°. These properties will become less reliable when greater amounts of noise are present in the data, but the results are sufficiently encouraging to suggest that the set of invariants proposed here might provide another approach to analysing MT data to complement the well-known tensor decomposition schemes currently in use.

ACKNOWLEDGMENTS

The authors thank Dr Alan G. Jones and an anonymous referee for their detailed and helpful comments, which resulted in a vastly improved paper. This investigation was started when the first author (JTW) was visiting Ted Lilley's geomagnetism group in the Research School of Earth Sciences, the Australian National University, and was continued in Adam Schultz's group at The Institute of Theoretical Geophysics, Cambridge University. He thanks both of them for making space and facilities available to him at these institutions during his sabbatical leave. Visiting Fellowships awarded by the Australian National University and St. Edmund's College, Cambridge, are also gratefully acknowledged. Thanks are due to the University of Victoria Computing Services for providing generous access to their IBM SP2 computer. This work is supported by research grants awarded by the Natural Sciences and Engineering Research Council of Canada and the University of Victoria.

REFERENCES

Agarwal, A.K. & Weaver, J.T., 1999. Magnetic distortion of the magnetotelluric tensor: a numerical study, *Earth Planets Space,* submitted.

Bahr, K., 1988. Interpretation of the magnetotelluric impedance tensor: regional induction and local telluric distortion, *J. Geophys.,* **62,** 119–127.

Bahr, K., 1991. Geological noise in magnetotelluric data: a classification of distortion types, *Phys. Earth planet. Inter.,* **66,** 24–38.

Berdichevsky, M.N. & Dmitriev, V.I., 1976. Basic principles of interpretation of magnetotelluric curves, in *Geoelectric and Geothermal Studies,* pp. 165–221, ed. Á. Ádam, KAPG Geophysical Monograph, Akademiai Kaido, Budapest.

Cox, C.S., Filloux, J.H., Gough, D.I., Larsen, J.C., Poehls, K.A., von Herzen, R.P. & Winter, R., 1980. Atlantic lithosphere sounding, *J. Geomag. Geoelectr.,* **32,** Suppl. I, 13–32.

Eggers, D.E., 1982. An eigenstate formulation of the magnetotelluric impedance tensor, *Geophysics,* **47,** 1204–1214.

Fischer, G. & Masero, W., 1994. Rotational properties of the magnetotelluric impedance tensor: the example of the Araguainha impact crater, Brazil, *Geophys. J. Int.,* **119,** 548–560.

Groom, R.W. & Bailey, R.C., 1989. Decomposition of the magnetotelluric impedance tensor in the presence of local three-dimensional galvanic distortion, *J. geophys. Res.,* **94,** 1913–1925.

Ingham, M.R., 1988. The use of invariant impedances in magnetotelluric interpretation, *Geophys. J. R. astr. Soc.,* **92,** 165–169.

Jones, A.G. & Groom, R.W., 1993. Strike angle determination from the magnetotelluric tensor in the presence of noise and local distortion: rotate at your peril!, *Geophys. J. Int.,* **113,** 524–534.

Larsen, J.C., 1977. Removal of local surface conductivity effects from low frequency mantle response curves, *Acta Geodaet., Geophys. et Montanist. Acad. Sci. Hung.,* **12,** 183–186.

Lilley, F.E.M., 1976. Diagrams for magnetotelluric data, *Geophysics,* **41,** 766–770.

Lilley, F.E.M., 1993a. Mohr circles in magnetotelluric interpretation (i) simple static shift; (ii) Bahr's analysis, *J. Geomag. Geoelectr.,* **45,** 833–839.

Lilley, F.E.M., 1993b. Three-dimensionality of the BC87 magnetotelluric data set using Mohr circles, *J. Geomag. Geoelectr.,* **45,** 1107–1113.

Lilley, F.E.M., 1993c. Magnetotelluric analysis using Mohr circles, *Geophysics,* **58,** 1498–1506.

Lilley, F.E.M., 1998a. Magnetotelluric tensor decomposition: 1. Theory for a basic procedure, *Geophysics,* **63,** 1885–1897.

Lilley, F.E.M., 1998b. Magnetotelluric tensor decomposition: 2. Examples of a basic procedure, *Geophysics,* **63,** 1898–1907.

Park, S.W. & Livelybrooks, D.W., 1989. Quantitative interpretation of rotationally invariant parameters in magnetotellurics, *Geophysics,* **54,** 1483–1490.

Ranganayaki, R.P., 1984. An interpretive analysis of magnetotelluric data, *Geophysics,* **49,** 1730–1748.

Smith, J.T., 1995. Understanding telluric distortion matrices, *Geophys. J. Int.,* **122,** 219–226.

Swift, C.M., 1967. Magnetotelluric investigation of an electrical conductivity anomaly in the southwestern United States, *PhD thesis,* Department of Geology and Geophysics, MIT, Cambridge, MA (reprinted in *Magnetotelluric Methods,* pp. 156–166, ed. Vozoff, K., Geophys. Reprint Ser. No. 5, 1988, SEG, Tulsa, OK).

Szarka, L. & Menvielle, M., 1997. Analysis of rotational invariants of the magnetotelluric impedance tensor, *Geophys. J. Int.,* **129,** 133–142.

Weaver, J.T., 1994. *Mathematical Methods for Geo-electromagnetic Induction,* Research Studies Press, Baldock.

Weaver, J.T., Agarwal, A.K. & Pu, X.H., 1999. Three-dimensional finite-difference modelling of the magnetic field in geoelectromagnetic induction, in *Three Dimensional Electromagnetics,* pp. 426–443, eds Oristaglio, M.J. & Spiess, B.R., *Geophysical Developments Series,* Vol. 7, SEG, Tulsa, OK.

Word, D.R., Smith, H.W. & Bostick, F.X., 1971. Crustal investigations by the magnetotelluric tensor impedance method, in *The Structure of Physical Properties of the Earth's Crust,* pp. 397–416, AGU Monograph No. 14 (reprinted in *Magnetotelluric Methods,* pp. 626–648, ed. Vozoff, K., Geophys. Reprint Ser. No. 5, 1988, SEG, Tulsa, OK).

Zhang, P., Roberts, R.G. & Pederson, L.B., 1987. Magnetotelluric strike rules, *Geophysics,* **52,** 267–278.